NASA CONTRACTOR
REPORT

Report No. 61313

EVALUATION OF ODYSSEY-I ORBITAL AERODYNAMIC EXPERIMENT PACKAGE

By W. P. Walters

Northrop-Huntsville
Huntsville, Alabama

July 1969

Prepared for

NASA-GEORGE C. MARSHALL SPACE FLIGHT CENTER
Marshall Space Flight Center, Alabama 35812

TABLE OF CONTENTS

TABLE OF CONTENTS (Concluded)

LIST OF ILLUSTRATIONS

LIST OF SYMBOLS

Symbol	Definition
A	Effective drag area
A/D	Analog to digital
AMU	Atomic mass unit
A/m	Ratio of effective drag area of satellite to its mass
a	Semimajor axis
a´	Defined in sketch page E-1
Δa	Semimajor axis change per orbital revolution
Al	Aluminum
Au	Gold
B	$\sqrt{2}\ \pi\ \sigma_c^2\ \frac{N_o}{W}$
b	$\frac{C_D\ A}{2m}$
b´	Defined in sketch page E-1
C_D	Drag coefficient
$C_{D_{fm}}$	Drag coefficient in free molecular flow
$C_{D_{nfm}}$	Drag coefficient in near free molecular flow
C_{D_I}	Drag coefficient due to momentum flux of incident molecules
C_{D_R}	Drag coefficient due to momentum flux of reflected molecules
COMP	Composition
D	Drag force
D´	Defined in sketch page E-1
d	Body diameter
d'	$\frac{\omega_s}{n}\ (1 - e^2)^{1/2}\ \cos i$
E	Perturbed eccentric anomaly
$\bar{E}$	Total kinetic flux of upper atmosphere
EUV	Solar extreme ultraviolet radiation
E_i	Incident particle energy

LIST OF SYMBOLS (Continued)

Symbol	Definition
E_r	Reflected particle energy
E_t	Energy that a particle would have if its temperature was completely accommodated to the surface temperature
e	Orbital eccentricity
$e^{'}$	Electron charge
ev	Electron volt
$F(S_b, S_\infty)$	Form of drag function for near free molecular flow defined in Appendix A ($F = F(S_b, S_\infty)$)
$\overline{F}$	Level of solar flux
F	Output frequency
f_1	Density scale height function, defined in text
f_2	Density scale height function, defined in text
$f(\nu, \text{shape})$	Function related to the nature of the gas-solid interaction and the body shape in Schamberg's model
G	Defined in text as equation (7)
GSI	Gas-surface interaction
h	Altitude measured from the earth's surface
I_r	Satellite roll moment of inertia
IR	Infrared
i^-	Electron current
i	Inclination angle
J	Defined in text as equation (8)
K_1, K_2, K_3	Parameters relating to the body geometry of the paddlewheel satellite and the particular gas-solid surface interaction model selected
Kn	Knudsen number defined as the ratio of the mean-free path of the molecules in question to an appropriate body dimension
$\overline{k}$	Frequency-Temperature dependence, dF/dT
k	Gravitational constant
L	Perpendicular distance from a paddle center to the spin axis
$L^{'}$	Distance between collector and edge of the electron beam

LIST OF SYMBOLS (Continued)

Symbol	Definition
M	Mean anomaly = E - e sin E
MST	Mountain standard time
MTOF	Metastable time of flight
m	Mass (appropriately designated in text)
N	Number of molecules striking target per unit area per second
N_2	Molecular nitrogen
N_o	Avogadro's number $\left(6.02 \times 10^{23} \frac{\text{molecules}}{\text{g mole}}\right)$
N'	Populations in the excited state
N'_o	Number of electrons in the excited state
n	Molecular number density
n_r	Number density of the re-emitted molecules
n_∞	Number density of the incident molecules
$\hat{n}$	Anomalistic mean motion
O	Atomic oxygen
O_2	Molecular oxygen
OGO	Orbital Geophysical Observatory
P	Period of orbital motion
P_o	Period of orbital motion defined in equation (9)
$\dot{P}$	Time rate of change of orbital period
p	Atmospheric pressure
Q	Net energy transfer in the form of heat
rps	Revolution per second
S	Speed ratio
S_b	Speed ratio of the satellite with respect to the most probable velocity of the molecules reflected from the body
S_∞	Speed ratio of the satellite with respect to the most probable velocity of the ambient freestream molecules
T	Temperature

LIST OF SYMBOLS (Continued)

Symbol	Definition
T_{ll}	Aerodynamic torque parallel to satellite spin axis
$T_{\perp}$	Aerodynamic torque perpendicular to satellite spin axis
T'	Transit time
T_i	Temperature of incident molecules
T_r	Temperature of reflected molecules
T_w	Temperature of molecules reflected from a wall at the wall temperature
TOF	Time of flight
t	Time
u	Perturbed argument of the satellite
v	Particle speed
V	Satellite velocity
V_i	Velocity of incident molecules with respect to the satellite surface
V_r	Velocity of reflected molecules with respect to the satellite surface
ΔV	small increment in velocity
W	Mean molecular weight
WC_p	Heat capacity
w	Defined in sketch page E-1

GREEK SYMBOLS

α or α_T	Thermal accommodation coefficient
α_D	Momentum accommodation coefficient
β	$\frac{\bar{i}\sigma^*}{\bar{e}\bar{a}}\eta_o$
δ	The angle between the normal to a paddle surface and the paddle-wheel satellite spin vector
η	The angle between the velocity vector and the paddlewheel satellite spin axis at perigee
η^*	Metastable density

LIST OF SYMBOLS (Concluded)

Symbol	Definition
n_o	Neutral particle density
θ	True anomaly in degrees
ϑ_i	Angle of incidence of molecules impinging on a surface
ϑ_r	Angle of reflection of molecules leaving a surface
ϑ' and ξ	Angles defined in text in equation (8)
μ	Sum of earth and satellite mass
ν	Exponent in equation (C-1) ranging from 1 to ∞
$\Delta\nu$	Spin-rate change per revolution
ρ	Atmospheric density
ρ_i	Density of incident flux
ρ_p	Atmospheric density at perigee
σ^*	Excitation cross section
$\sigma^*/\delta a'$	Probability of excitation per unit time
$\bar{\tau}$	Paddlewheel torque averaged over a spin cycle
τ	Mean residence time in excited state
$\Phi(\phi_o)$	The ratio of the axial component of momentum carried away from a surface to the momentum which would have been carried away if all the reflected molecules were aligned with the axis of the reflected beam
ϕ	Defined in Figure C-1
ϕ_o	Defined in Figure C-1
ω_s	Planetary rotation rate
$\delta a'$	Defined in sketch page E-1
δW	Defined in sketch page E-1
δV	Elemental volume

NOTE: Units are used in the text only where necessary for clarity. The reader may insert consistent units as needed.

SUMMARY

The ODYSSEY I experiment package is reviewed in regard to its ability to survey the earth's upper atmosphere. In particular, the ODYSSEY I experiments are designed to determine satellite drag coefficients, gas-solid surface interaction phenomena and other pertinent aerodynamic parameters. Also, other aerodynamic or aeronomy orbital experiments similar in nature to those of the ODYSSEY experiments will be reviewed.

The ODYSSEY I experiment package described in this report includes, as a basis, the Paddlewheel/Diffuse Sphere experiment, a gas-solid surface interaction experiment and a mass spectrometer. This experiment package is shown to be capable of determining the following data at a nominal 160 to 200 km perigee altitude:

- The free-molecular-flow aerodynamic drag coefficient of spheres and flat plates, using typical engineering bodies under orbital energy conditions.
- The thermal accommodation coefficient of typical satellite surfaces under orbital energy conditions.
- Information directly related to the nature of the gas-solid surface interaction phenomena through a detailed study of the velocity distributions of the incident and reflected gas beams.

Additional data obtained by the experiment package will consist of:

- The incident molecular flux and absolute mass density.
- The number densities of the neutral constituents of the atmosphere in the stated altitude range.

The addition of another experiment (e.g. the Passive Drag Sphere Ensemble) would allow data to be obtained relevant to the following:

- The near-free-molecular-flow aerodynamic drag coefficient of typical engineering surface spherical satellites.
- The higher order terms in the expansion of the earth's gravitational potential and the determination of exact tracking station locations.

Some of the other relevant aerodynamic and aeronomy experiments are reviewed and are found to have certain capabilities which might supplement or enhance the ODYSSEY I Project.

Section I

INTRODUCTION

Present knowledge of the earth's upper atmosphere and its temporal and spatial variations has been obtained largely by observing the orbits of artificial earth satellites. However, the observation of one satellite orbiting alone provides only the product of the density and the aerodynamic drag coefficient (i.e., ρC_D). In order to separate the drag coefficient, C_D, from the density, ρ, additional information is required as outlined in this report. Detailed understanding of the satellite aerodynamic drag coefficient, the nature of the gas-solid surface interaction phenomenon, and the velocity distributions of the incident and reflected molecular flux is very poor in this altitude range. This uncertainty in both the near-free and free-molecular-flow drag coefficients is further complicated by the fact that the drag coefficient, distribution of the molecular flux, and the gas-solid surface interaction phenomenon are all interrelated.

The altitude range considered in these studies is the critical 130 to 240 km range where aerodynamic forces become significant and where departure from free molecular flow begins for typical satellites. In addition, the determination of the variability of the atmospheric parameters is considered important in this altitude range because processes which determine the structure of the upper atmosphere occur throughout this region. Unfortunately, existing model atmospheres are deficient in this altitude range, especially regarding the extreme limits and variability of the absolute density and composition.

The major uncertainty in determining satellite drag coefficients and thermal accommodation coefficients in the 130 to 240 km altitude range is related to the uncertainty in determining the composition and absolute density of the atmosphere in this altitude range. This uncertainty is due to the inability of experimenters, using in situ instrumentation, to obtain a quantitative measurement of atomic oxygen. Thus, it is recommended that further laboratory studies

be conducted to investigate new methods of producing and detecting atomic oxygen. Also, a strong recommendation is made to encourage experimenters interested in the 130 to 240 km altitude range to organize their efforts further in order to maximize the effectiveness of future aerodynamic and certain aeronomy experiments.

In addition, the effects of geomagnetic storms and solar activity on temporal density variations are relatively unknown in the altitude range below 200 km. This is due to the relatively short lifetime of satellites below 240 km and to the smoothing effects on density determinations resulting from observations of orbital decay only. Thus, diurnal and other short-term density variations have not been determined with confidence. Measurements of atmospheric composition have been obtained with even less confidence due to the limitations of in situ instrumentation used to date. As an example of the problems concerned with composition determination, mass spectrometer measurements conducted near 120 km have implied a ratio of atomic oxygen to molecular oxygen number densities ranging from 1 to 4 (von Zahn, 1967, ref. 1). Also, Kasprzak, et al., 1968 (ref. 2) and Krankowsky, et al., 1968 (ref. 3) have shown that existing spreads in the measured data are due in part to the loss of atomic oxygen by trapping at the instrument's walls and recombination in the region of the ion source. Thus, a large error band exists in determination of satellite drag coefficients directly from orbital tracking data due to the uncertainty in the absolute measurement of atmospheric density.

The following sections discuss the limitations in the present knowledge of the structure of the upper atmosphere and in orbital aerodynamics. In particular, a description is given of the state of the art in the prediction of environment induced orbital dynamics. Present model atmospheres are discussed from the viewpoint of their limited prediction capabilities and a discussion is given of the ability of experimenters to predict aerodynamic drag. The ODYSSEY I experiment is introduced as an ambitious satellite program designed to remove some of the present uncertainties regarding satellite drag coefficients and other related aerodynamic phenomenon.

This report also includes a section describing a few other aeronomy and aerodynamic experiments that have been completed or proposed and which are of interest to the ODYSSEY experiment planners.

Section II
SATELLITE ENVIRONMENT INDUCED ORBITAL DYNAMICS AND KNOWLEDGE OF THE EARTH'S ATMOSPHERE

2.1 ENVIRONMENT INDUCED ORBITAL DYNAMICS

Scientific satellites in this decade have been affected adversely by the lack of knowledge concerning the gas-surface interaction and the absolute atmospheric density even though their operational altitude was far above what was normally thought to be the region of significant aerodynamic forces. For example, Ariel II had a lifetime of only 140 days whereas 540 days were predicted (Ariel II, 1965, ref. 4; Stewart and Miller, unpublished, ref. 5). Because of the lowered spin rate and attitude drift, some of the experiments became intermittent or inoperative after approximately 90 days. In another example, the designers of the first paddlewheel satellite, Explorer VI, expected the momentum of the air molecules reemitted by the satellite surfaces to be described by Maxwell's classical model with approximately 95 percent of the molecules diffusely reflected. The spin actually decayed three times as fast as expected, and an order of magnitude faster than would have occurred if the reemission had been completely accommodated (Reiter, unpublished, ref. 6).

Aerodynamic torques can be significant on some satellites even at altitudes approaching 1000 km. This is especially true on spin satellites such as Alouette II (Vigneron and Garrett, 1967, ref. 7) which is an ionspheric sounding instrument having a small diameter (0.5 in.) tubular antenna. The antenna is a crossed dipole measuring 240 and 75 feet tip-to-tip. The uneven heating of the antenna and subsequent distortion in the antenna shape has resulted in uneven aerodynamic forces and undesirable spin decay. Alouette II's orbit is 500 to 3000 km and should experience even greater aerodynamic forces during the forthcoming period of high solar activity (the satellite was launched on 28 November 1965). A comparison of the predicted atmospheric drag pressure on Alouette II is shown in Figure 2-1 for average conditions of solar activity and for conditions of maximum sunspot activity. The authors (Vigneron and Garrett, 1967, ref. 7) expect the higher altitude satellite, Alouette I, to experience significant atmospheric drag effects during periods of high solar

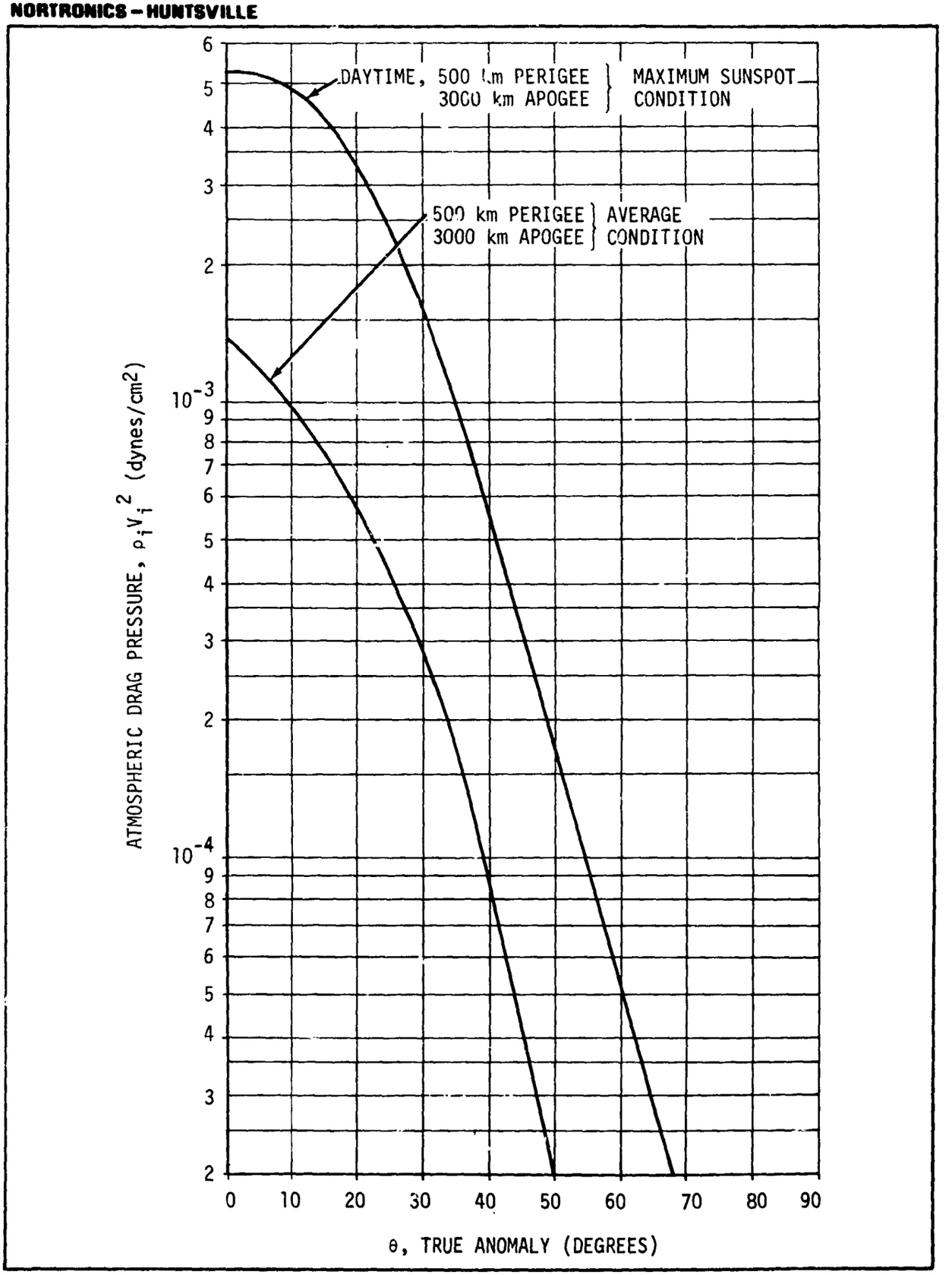

Figure 2-1. PREDICTED ATMOSPHERIC DRAG PRESSURE VS TRUE ANOMALY ON A SURFACE PERPENDICULAR TO THE VELOCITY VECTOR (ALOUETTE II SATELLITE, REF. 7)

activity even though the perigee altitude is near 1000 km. They have predicted that the atmospheric drag pressure will be one to two orders of magnitude larger than that corresponding to low solar activity.

Orbital spacecraft now in the planning and design stages are far more sophisticated than earlier satellites. Their mission requirements place severe limitations on spacecraft designers and mission planners due to the specification of extremely long orbital lifetimes, precise and continuous attitude control, and increased size and complexity. Examples of such highly complex spacecraft are the NASA S-IVB Orbital Workshop and the Air Force Manned Orbiting Laboratory. These and other new generation spacecraft have stringent requirements for long orbital lifetimes and will place severe demands on the attitude control systems.

For such spacecraft it is no longer sufficient to merely assume an aerodynamic coefficient of drag equal to 2.2 and to assume that the maximum atmospheric density predicted by the present models (CIRA, 1965, ref. 8 and USSAS, 1966, ref. 9) is the most conservative and safe value to use. Recent data (King-Hele and Quinn, 1966, ref. 10) of night-to-day atmospheric density variation have shown that, in the 170 to 210 km altitude range, the CIRA 1965 model atmosphere (ref. 8) predicts too small a diurnal variation. Shortcomings of the present model atmospheres are described in considerable detail in this report (subsection 2.2) and elsewhere in the literature (e.g. Priester, 1965, ref. 11; King-Hele and Quinn, 1966, ref. 10). Part of the uncertainty in published atmospheric densities can, of course, be attributed to uncertainties in the evaluation of the coefficients of drag. However, even these uncertainties cannot completely explain the disagreement between the present model atmospheres and the drag-deduced densities since Cook, 1965, (ref. 12) concluded that the uncertainty in the aerodynamic drag coefficient for a spherical satellite cannot exceed $\pm$ 30 percent and is probably less than $\pm$ 10 percent at 280 km. From an engineering standpoint, the worst consequence of not knowing accurately the absolute atmospheric density and the gas-surface interactions present is that attitude-control torques cannot be properly estimated; thus, the cold-gas thruster systems and torque wheels of the large observatory-type satellites must be over-designed if failure part-way through a mission is to be

prevented (Moe, 1967, ref. 13). This lack of knowledge can be of consequence to a successful mission at altitudes of 300 km and above and can severely limit successful mission completion at altitudes below 300 km.

2.2 PREDICTION OF PARAMETERS USING MODELS OF THE ATMOSPHERE

The most recent model atmospheres are the Cospar International Reference Atmosphere (CIRA 1965, ref. 8) and the U. S. Standard Atmosphere Supplement (USSAS 1966, ref. 9). Both of these atmospheric models are based on exospheric parameters which have been obtained mainly from observation of satellite drag. The models use lower boundary conditions at 120 km based mainly on the drag data obtained from observation of falling spheres (Bartman, et al., 1956, ref. 14; Faire and Champion, 1965, ref. 15; Faucher, et al., 1963, ref. 16; and Peterson, et al., 1965, ref. 17). The CIRA 1965 model assumes the boundary conditions at 120 km to be constant regardless of hour, season, or latitude. A significant improvement to the 1962 U. S. Standard Atmosphere (NASA, 1962, ref. 18) was accomplished by fitting the exospheric values at 120 km to three different starting points designated winter, summer, and mean. These improvements have been incorporated into the latest model atmosphere (USSAS, 1966). A great need for verification of these models is evident especially when one considers the detrimental effects on satellite orbital and operational lifetimes resulting from inadequate predictions of atmospheric density.

Observational values of air density and composition at heights of 130 to 240 km are extremely sparse and allow only poor correlation with latitudinal variations and day-to-night, seasonal, and other temporal variations. This altitude range (130-240 km) is the region of interpolation from densities and temperatures determined from falling sphere drag data below 120 km and from relatively long-life orbital satellites above 200 km. Observational values at times of high solar activity are virtually nonexistent. Figure 2-2 represents a sampling of air density values obtained from the orbital decay of satellites (King-Hele and Quinn, 1966, ref. 10), nighttime densities obtained by mass-spectrometer measurements (Hedin and Nier, 1966, ref. 19), daytime densities determined by extreme ultraviolet absorption measurements (Hall, et al., 1965, ref. 20), and Model 2 of the CIRA 1965 model atmosphere (ref. 8). The

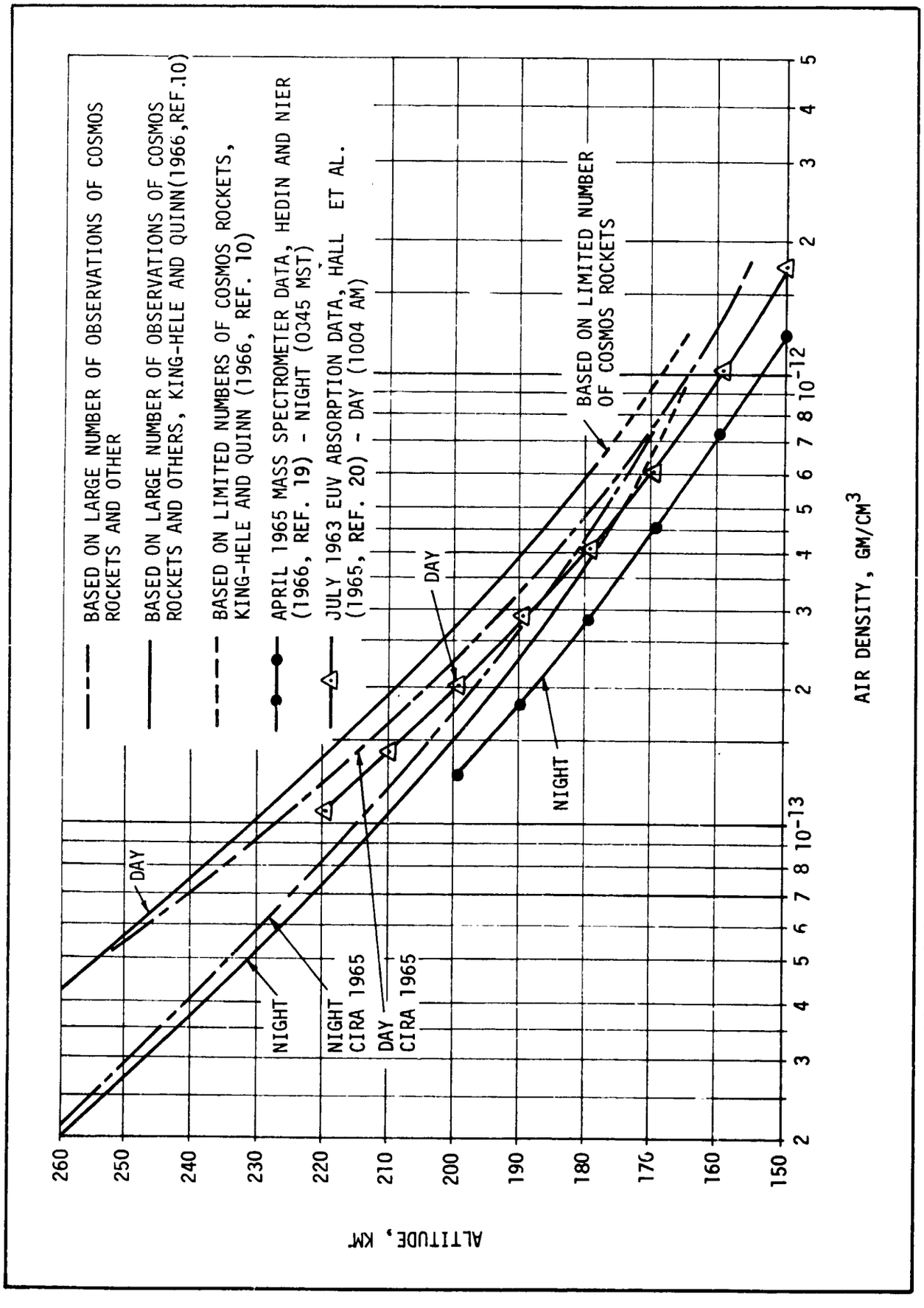

Figure 2-2. DAYTIME AND NIGHTTIME AIR DENSITIES AT 160-250 KM IN THE YEARS OF LOW SOLAR ACTIVITY 1962-5

model atmosphere curves plotted (day-1400 hours; night-0400 hours) represent the period of low solar activity from mid-1963 to 1965 ($\overline{F}$ = 75) which corresponds to the period in which the in situ measurements were taken. Based on a comparison between the densities determined by the recent satellite decay observations (Figure 2-2) and Model 2 of CIRA 1965, King-Hele and Quinn, 1966, (ref. 10) make the following conclusions:

- The CIRA 1965 daytime and nighttime variation is probably too small for heights of 170-200 km.
- Observational values of absolute atmospheric densities are entirely too sparse in the 150-170 km range to link up with the density values below 150 km.

Also shown in Figure 2-2 are the results of two direct measurements of density by instrumented rocket flights. The nighttime data represent mass spectrometer measurements made from an Aerobee rocket (NASA 4.127 UA) flown over White Sands Missile Range, New Mexico, on 5 April 1965, at 0345 MST (Hedin and Nier, 1966, ref. 19). The daytime data represent extreme ultraviolet absorption (EUV) measurements obtained from a rocket flight, also over White Sands, New Mexico, on 10 July 1963, at 1004 a.m. local time (Hall, et al., 1965, ref. 20). The nighttime data are lower than the model atmosphere data by a factor of approximately 1.5 and are typical of similar comparisons (Horowitz, 1966, ref. 21). The EUV absorption measurement is encouragingly close to the daytime value of the model atmosphere and is in reasonable agreement with the orbital decay observations of King-Hele and Quinn, 1966, (ref. 10) above approximately 190 km. However, there has not been a sufficient number of EUV absorption measurements to establish their validity.

Figure 2-3 contains some of the more recent N_2 number density values determined by the MUMP (Marshall Space Flight Center-University of Michigan Probes) mass spectrometer flights. The MUMP instrumentation consisted of an Omegatron mass spectrometer flown on a Nike-Tomahawk sounding rocket. The primary objective of the MUMP test series was to provide neutral N_2 density data for one diurnal cycle on January 24, 1967. Additional data were obtained at predicted times of the maximum and minimum of the diurnal variation on

April 25, 1967. The altitude range spanned by the MUMP test series was 140 to 320 km. In addition to the N_2 number densities obtained by this test series, temperature data, electron densities, and electron temperature data were also obtained. In all, a total of eight MUMP shots were utilized.

Figure 2-3 presents the N_2 number density profiles for the MUMP 1 (Daytime-Maximum) and MUMP 8 (Nighttime-Minimum) data.

The major conclusions of the MUMP test series are summarized as follows (Taeusch, et al., 1967, ref. 22):

- The N_2 number densities deduced from satellite drag measurements are usually about a factor or two higher than those determined by conventional gauge and mass spectrometer techniques.
- The CIRA 1965 model atmosphere nighttime temperatures are in good agreement with the direct measurements, but the daytime model temperatures are consistently too high at the level of solar activity used for comparison.
- The atmospheric temperatures and densities below 200 km are more variable than the current atmospheric models predict.
- The MUMP mass spectrometer results are consistent with the Jacchia empirical formulae, which predicts exospheric temperature as a function of geomagnetic activity, solar flux, and time of the day and year.

Additional information on the MUMP test series is available from references 22, 23, and 24.

Figures 2-4, 2-5, 2-6, and 2-7 present some of the most recent particle number densities and total mass densities from 120 to 220 km. These data were obtained by Kasprzak, et al., Nov. 1968 (ref. 2) and Krankowsky, et al., Dec. 1968 (ref. 3). The data from ref. 2 utilized two Aerobee rocket flights over White Sands, New Mexico (32° 24'N, 106° 20.6' W) November 30, 1966 at 0445 MST and December 2, 1966 at 1409 MST. Three magnetic deflection mass spectrometers were employed on each flight to measure day-night effects in the atmosphere and the N_2, O_2, O, Ar and He number densities. One mass spectrometer had an open ion source to minimize the number of collisions between the atmospheric constituents and the instrument surfaces before reaching

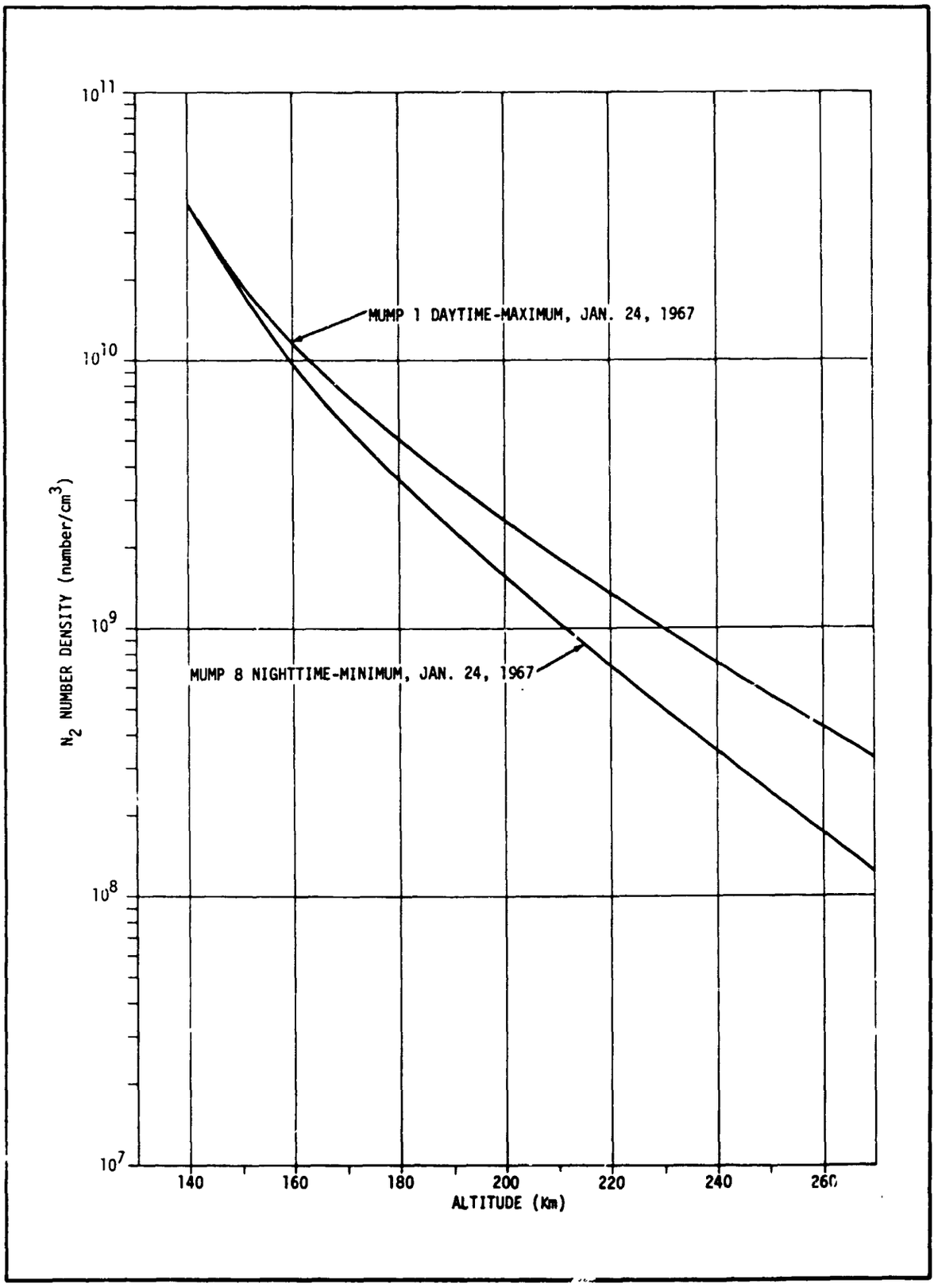

Figure 2-3. VARIATION OF N_2 NUMBER DENSITY WITH ALTITUDE FOR TWO SELECT MUMP MASS SPECTROMETER FLIGHTS (TAUESCH ET AL., 1967, REF. 22)

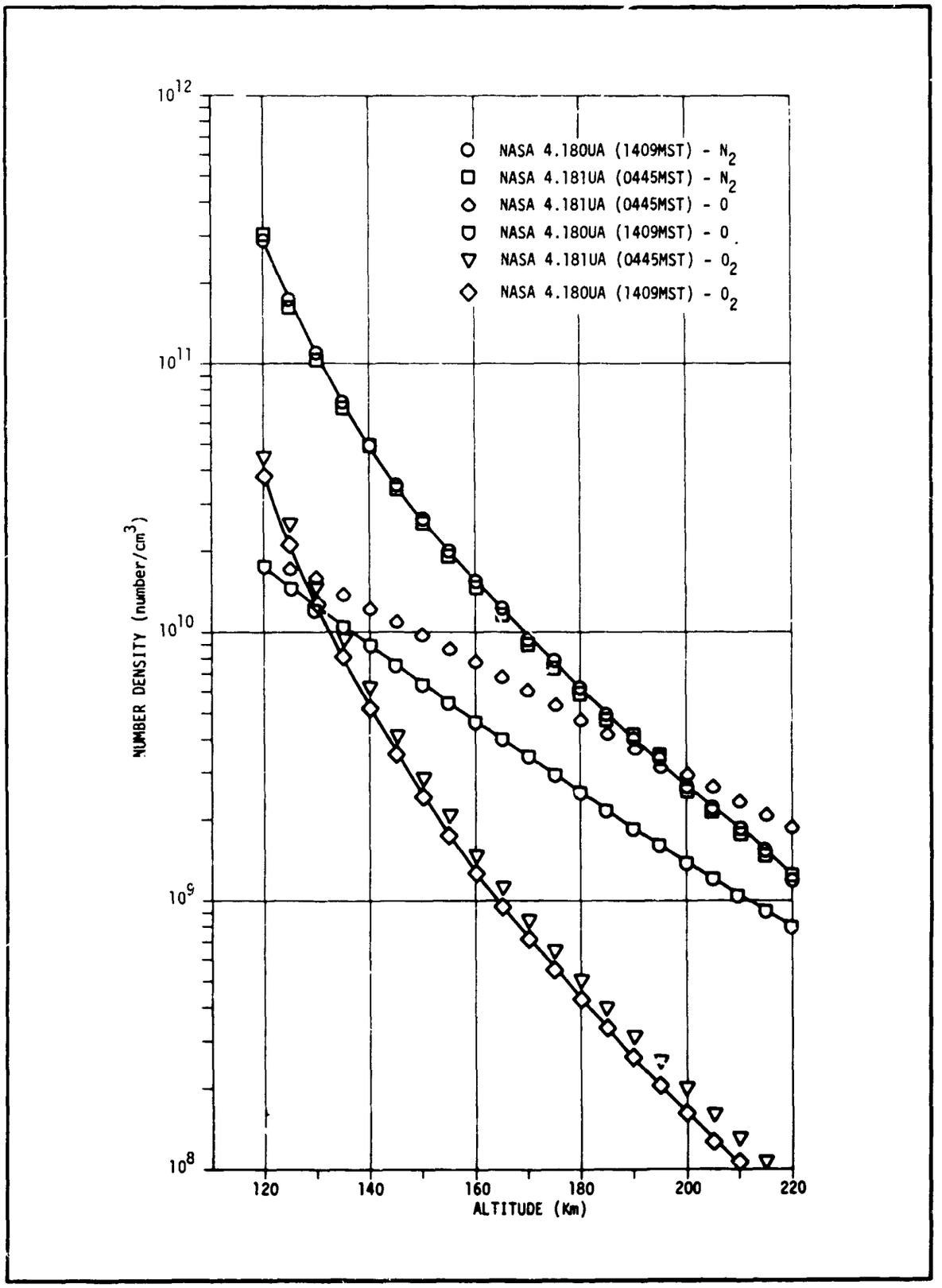

Figure 2-4. PARTICLE NUMBER DENSITY VARIATION WITH ALTITUDE FOR TWO MASS SPECTROMETER FLIGHTS OVER WHITE SANDS, NEW MEXICO, 1966 (KASPRZAK ET AL., 1968, REF. 2)

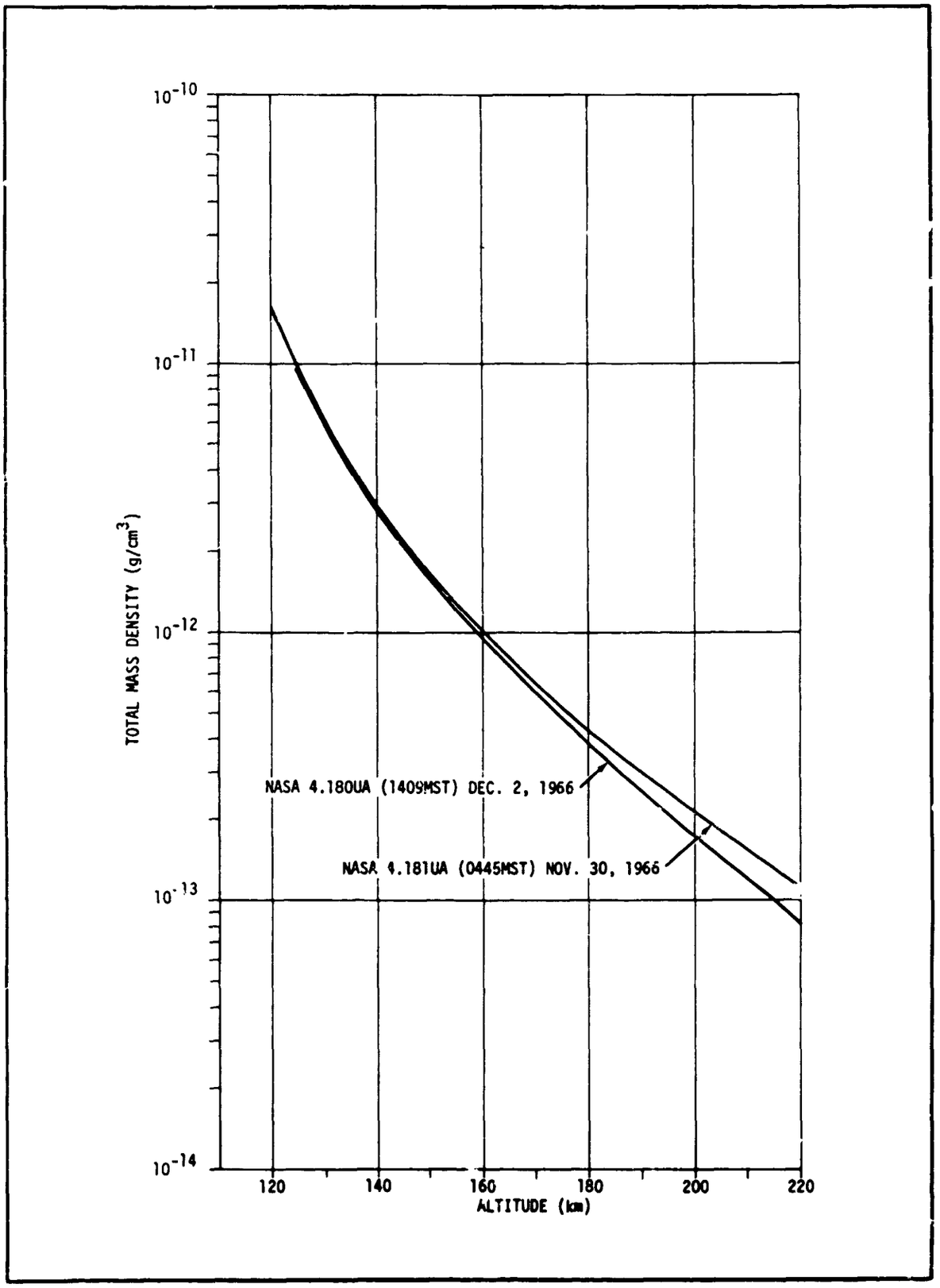

Figure 2-5. TOTAL MASS DENSITY VARIATIONS WITH ALTITUDE FOR TWO MASS SPECTROMETER FLIGHTS OVER WHITE SANDS, NEW MEXICO, 1966 (KASPRZAK ET AL., 1968, REF. 2))

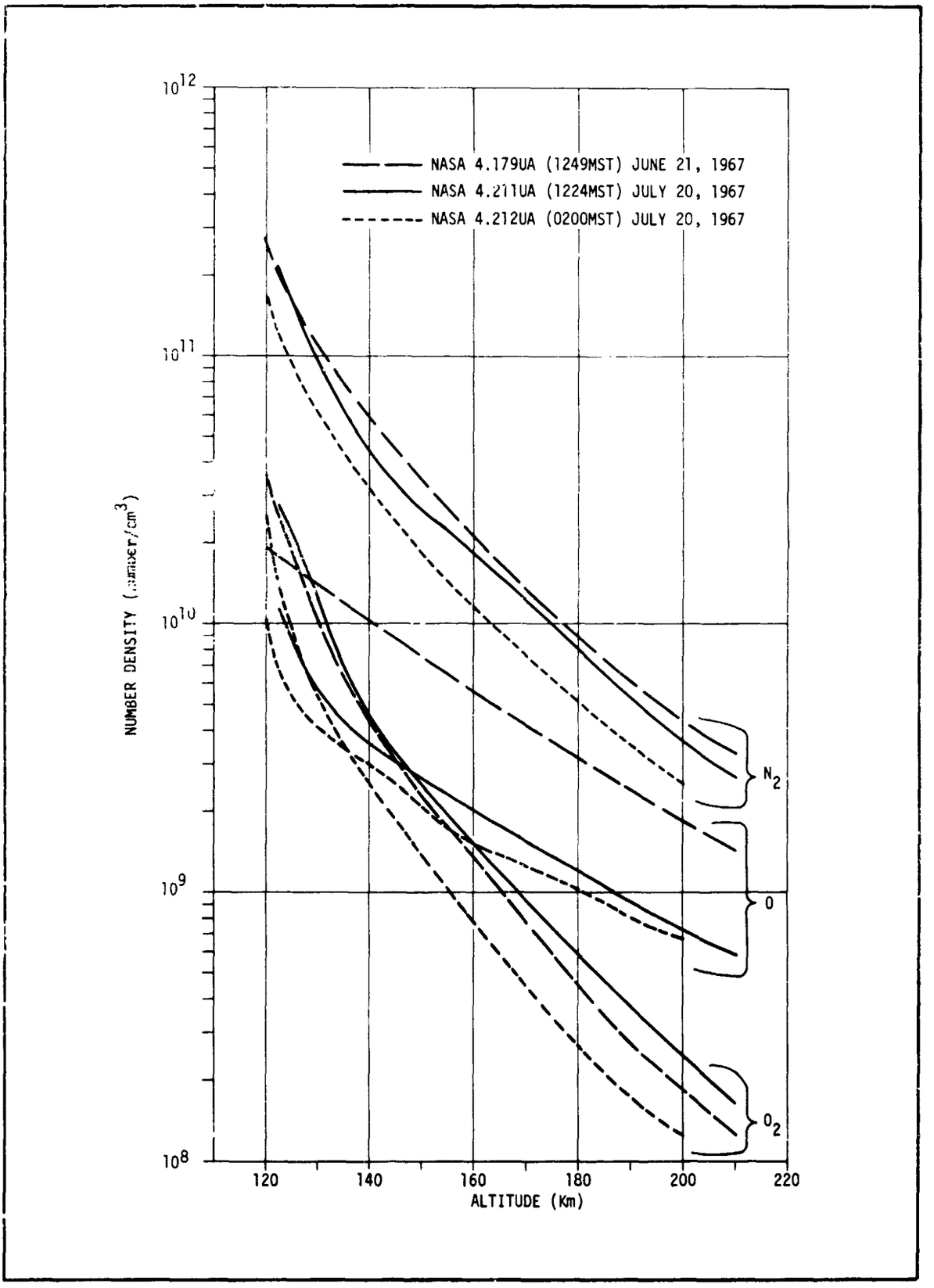

Figure 2-6. PARTICLE NUMBER DENSITY VARIATION WITH ALTITUDE FOR THREE MASS SPECTROMETER FLIGHTS OVER WHITE SANDS, NEW MEXICO, 1967 (KRANKOWSKY ET AL., 1968, REF. 3))

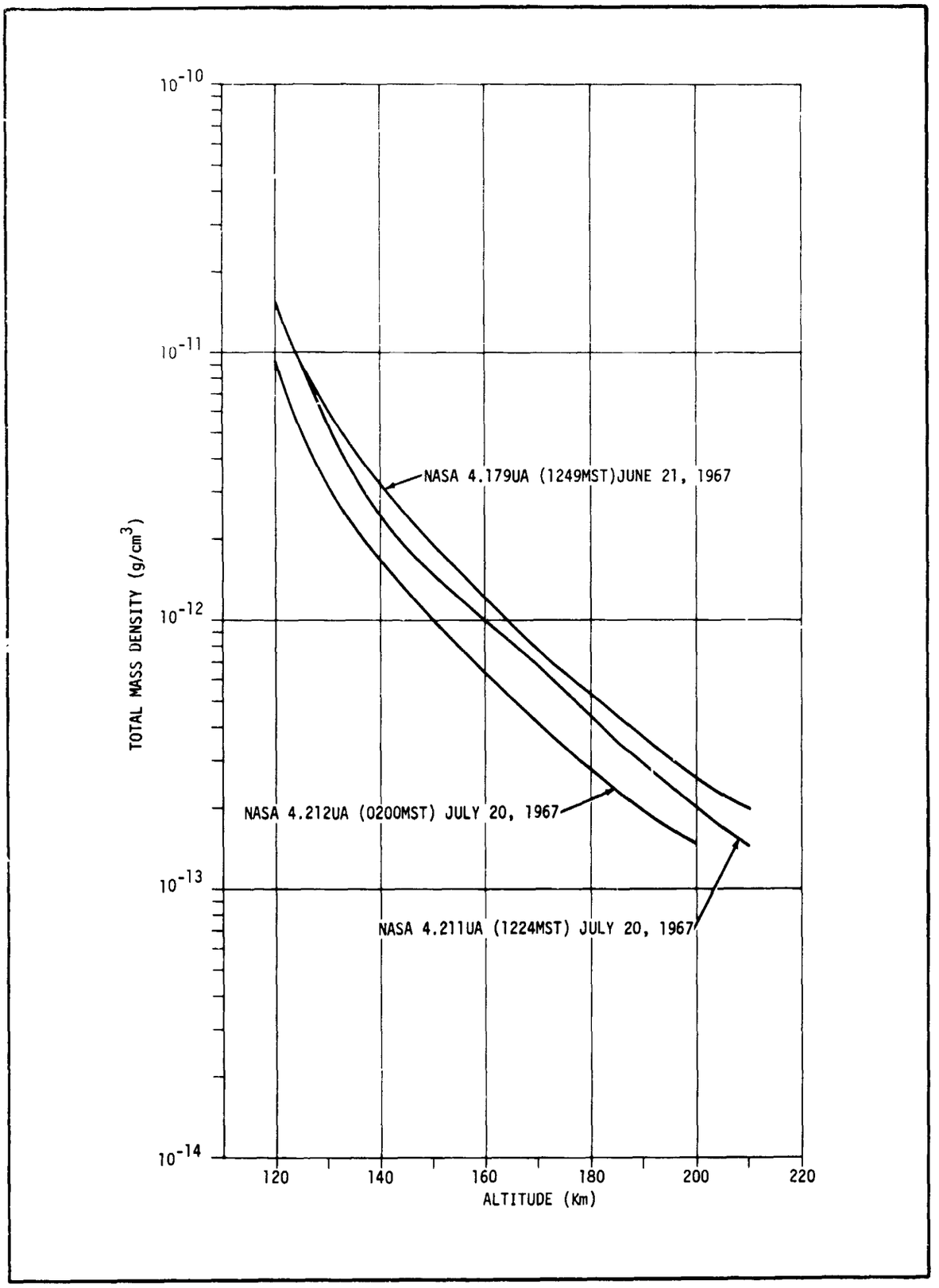

Figure 2-7. TOTAL MASS DENSITY VARIATIONS WITH ALTITUDE FOR THREE MASS SPECTROMETER FLIGHTS OVER WHITE SANDS, NEW MEXICO, 1967 (KRANKOWSKY ET AL., 1968, REF. 3)

the ionization region. The other two mass spectrometers had their ion sources enclosed in a cavity, connected to the ambient atmosphere by a telescoping cylinder. One of these closed ion source mass spectrometers measured only N_2.

Figure 2-4 presents the N_2, O_2, and O number density profiles from ref. 2. The data from both rocket flights are compared in this figure. The atomic oxygen (O) profiles presented here assume no wall loss. If total surface loss were assumed for O, the ambient O number densities would be higher by about a factor of 5. This difference in O concentration is revealed by the difference in the O readings between the open and closed ion source mass spectrometers (Kasprzak, et al., Nov. 1968, ref. 2). However, the loss coefficient is believed to be much closer to zero, as plotted in Figure 2-4, than it is to one (ref. 2). On the other hand, loss coefficients of nearly one were assumed for the MUMP data, ref. 25. Thus, a great deal of uncertainty concerning the number density of O still exists.

Figure 2-5, also from ref. 2, shows the total mass density profiles for both rocket flights deduced from the mass spectrometer number density measurements. The reader is referred to ref. 2 for further details.

Figure 2-6 presents N_2, O_2, and O number density profiles from three rocket flights over White Sands, New Mexico (32° 24'N, 106° 20.6'W) at 1249 MST June 21, 1967, and at 0200 MST and 1224 MST July 20, 1967, (Krankowsky, et al., Dec. 1968, ref. 3). Each rocket carried three mass spectrometers of the same type and collected the same type of data as discussed in the preceding paragraphs, (ref. 2).

The purpose of these experiments was to study the diurnal variations in the composition of the atmosphere from 120 to 200 km and to extend the data of Kasprzak, et al., Nov. 1968 (ref. 2) to a different season. Again, as in ref. 2, the atomic oxygen is based on a zero loss coefficient. The effects of assuming a loss coefficient other than zero are discussed in ref. 3.

Figure 2-7 shows the total mass densities derived from the three rocket flights (ref. 3). Further details as well as additional density comparisons and temperature profiles are given in Krankowsky, et al., Dec. 1968 (ref. 3).

Krankowsky, et al., Dec. 1968, ref. 3, compared their test results with the U. S. Standard Atmosphere Supplements 1966 (summer model, ref. 9). The disagreement between the measurements and the model predictions were striking except for the N_2 number densities for the two daytime flights, 4.179 and 4.211, which showed good agreement with the model. For all flights the O_2 and O number densities were lower than the model predictions. Also the present measurements suggest variable number densities for all constituents at 120 km whereas the model atmospheres do not. Additional discussion of the data is available in ref. 3.

Figure 2-8 compares the total mass density profiles for the five rocket flights of references 2 and 3. Basically, the June 21, 1967, at 1249 MST flight represents, for the most part, the highest number density. The July 20, 1967, at 0200 MST flight represents the lowest number density (see ref. 3). As Figure 2-8 points out, rocket flights 4.181 and 4.180 indicate a day-to-day density variation at these altitudes and time of year. This variation is of the same order of importance as the diurnal effects. These two effects are of an opposing nature, since the N_2 and O_2 number densities were unchanged from day to night but the nighttime O number density was higher than its daytime value. It seems that the day-to-night variations in the atmospheric composition are larger than current models predict. However, the diurnal effects suggested by the models may not be the only cause of day-to-night variations in the upper atmosphere. Changes may occur from day-to-day enhancing or cancelling diurnal variations (refs. 2 and 3).

Thus, recent atmospheric density measurements do not agree with the current atmospheric models. In order to derive an accurate model, it is necessary to determine density profiles for both spatial and temporal variations. Very little density data exists in altitude ranges below 240 km for periods of high solar activity, and conditions above 240 km are derived from density profiles determined by satellite drag measurements. The density is determined indirectly

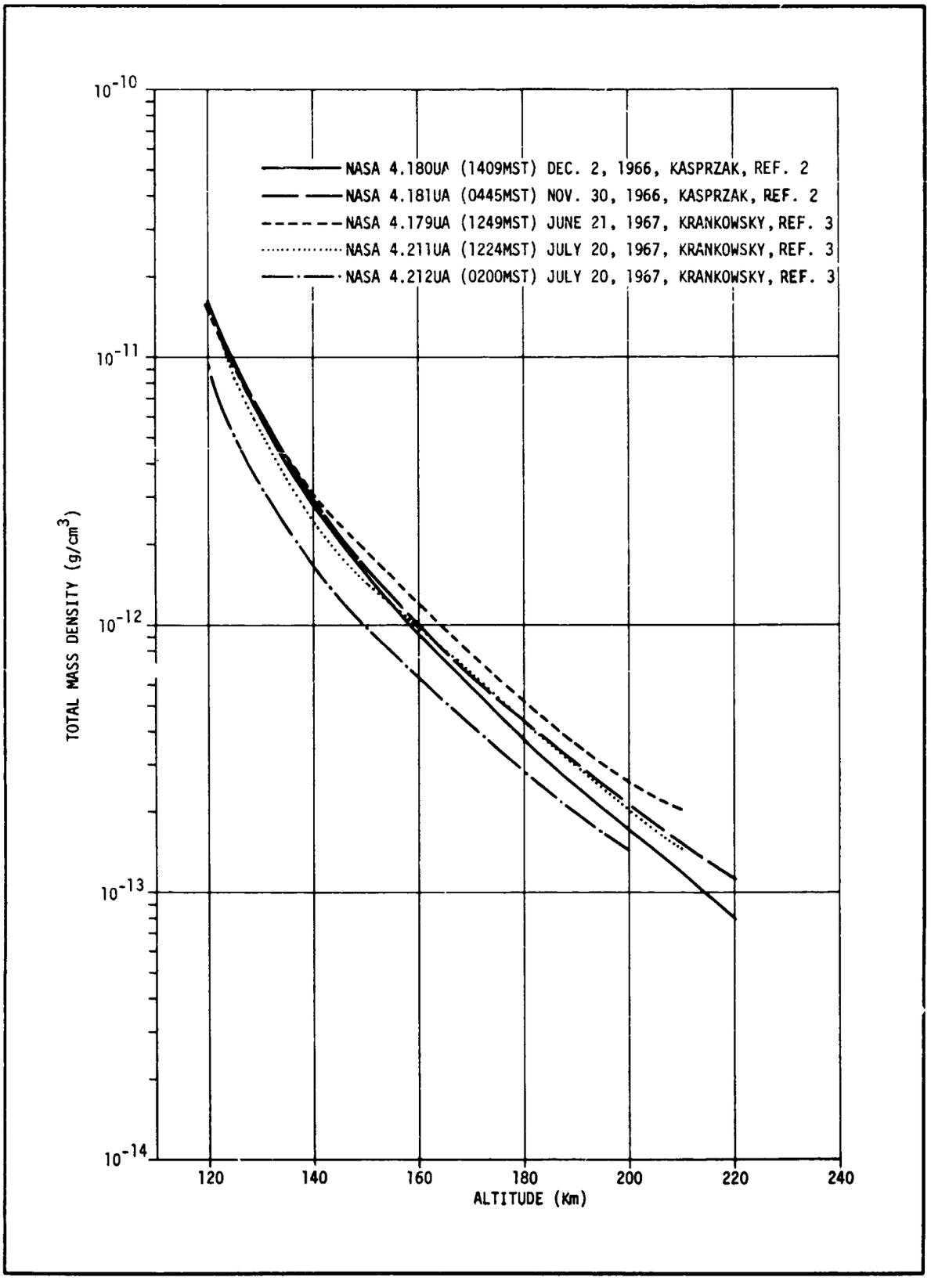

Figure 2-8. COMPARISON OF FIVE MASS SPECTROMETER TOTAL MASS DENSITY MEASUREMENTS VERSUS ALTITUDE

with temperature and composition being based on density model calculations. Model calculations, in turn, depend on the assumed atmospheric conditions at a reference level of approximately 120 km. This reference level is assumed because rocket vapor experiments indicate that somewhere near this altitude range convective mixing switches to diffusive mixing. Thus, the structure of the upper atmosphere above 200 km depends on the temperature and composition of the atmosphere between 100 and 200 km.

The region between 100 and 200 km has been probed by a number of rockets which have yielded information concerning instantaneous composition and density at one particular point. From these experiments, wide variations in atmospheric properties have been observed. For example, either spatial or temporal inhomogeneity in the atmosphere has caused the number density of atomic oxygen, deduced by rocket measurements at 120 km, to vary by a factor of four (von Zahn, 1967, ref. 1). See also Kasprazak, et al., Nov. 1968 (ref. 2), and Krankowsky, et al., Dec. 1968 (ref. 3). Only by direct observation over extended periods of time will it be possible to determine whether the heat introduced into the atmosphere by the absorption of ultraviolet radiation is convected, conducted, or radiated throughout the atmosphere. Also, these direct observations will determine whether or not photochemical association is coupled with diffusion, an important process in determining the upper atmospheric structure.

Satellite drag observations have revealed a time variation of density. It is generally assumed that these fluctuations are caused by variations in the intensity of the ultraviolet radiation from the Sun. Ultraviolet radiation with a wavelength of 1750Å is gradually absorbed within the atmosphere at heights below 200 km. It is assumed that changing thermal conditions within the 100 to 200 km altitude region produce the observed fluctuations in density at higher levels. However, it is not clear that changes in the ultraviolet radiation are solely responsible for fluctuations within the 100 to 200 km region. For example, gravity waves could be absorbed within this altitude range causing a portion of the heat absorption (Cannon, et al., 1966, ref. 26). These gravity waves are generated in the lower atmosphere and propagate upward before being absorbed in the rarefied gases at heights above 100 km. Again,

only a direct determination of density within the 100 to 200 km region will permit a determination of the contribution of the lower atmosphere to the thermal balance of the upper atmosphere.

Thus, the uncertainty in the model atmospheres for the range of approximately 100 to 200 km originates from the following problems:

- The orbital lifetime of most satellites is relatively short in this altitude range producing sparse and inconsistent results.
- Direct in situ measurements in this altitude range have been entirely too few to adequately correlate with atmospheric conditions.
- Uncertainties in the absolute values of the densities and compositions determined by instruments have not been satisfactorily resolved.
- Uncertainties exist in the applicable value of the aerodynamic coefficient of drag, C_D, to be used in preparation of model atmospheres. The aerodynamic drag coefficients of interest in high altitude studies are the near-free- and free-molecular-flow drag coefficient values.

2.3 PREDICTION OF AERODYNAMIC DRAG

Free molecular flow exists when ambient atmospheric molecules which lie in a satellite's path have a nearly perfect chance of passing through the cloud of molecules reflected by the satellite without a collision. Free molecular flow is attained when a mean free path, based on a representative density of the scattered cloud and on a collision cross section appropriate to intermolecular encounters at satellite speeds, is much greater than the diameter of the satellite. In this region, a further reduction in density produces no important changes in C_D.

Nominal values of satellite aerodynamic drag coefficients are shown in Figure 2-9 taken from Cannon, et al., 1966 (ref. 26). Extreme bounds on the values are included. This plot was obtained from satellite free-molecular-flow measurements and low-density tunnel, near-free-molecular-flow measurements for $0.001 \leq Kn \leq 1.5$. Basically, most of the free-molecular-flow aerodynamic drag is due to the incident momentum flux delivered to the satellite and is denoted here as C_{D_I}, the coefficient of drag due to the incident molecules. For spherical satellites this drag coefficient is given by

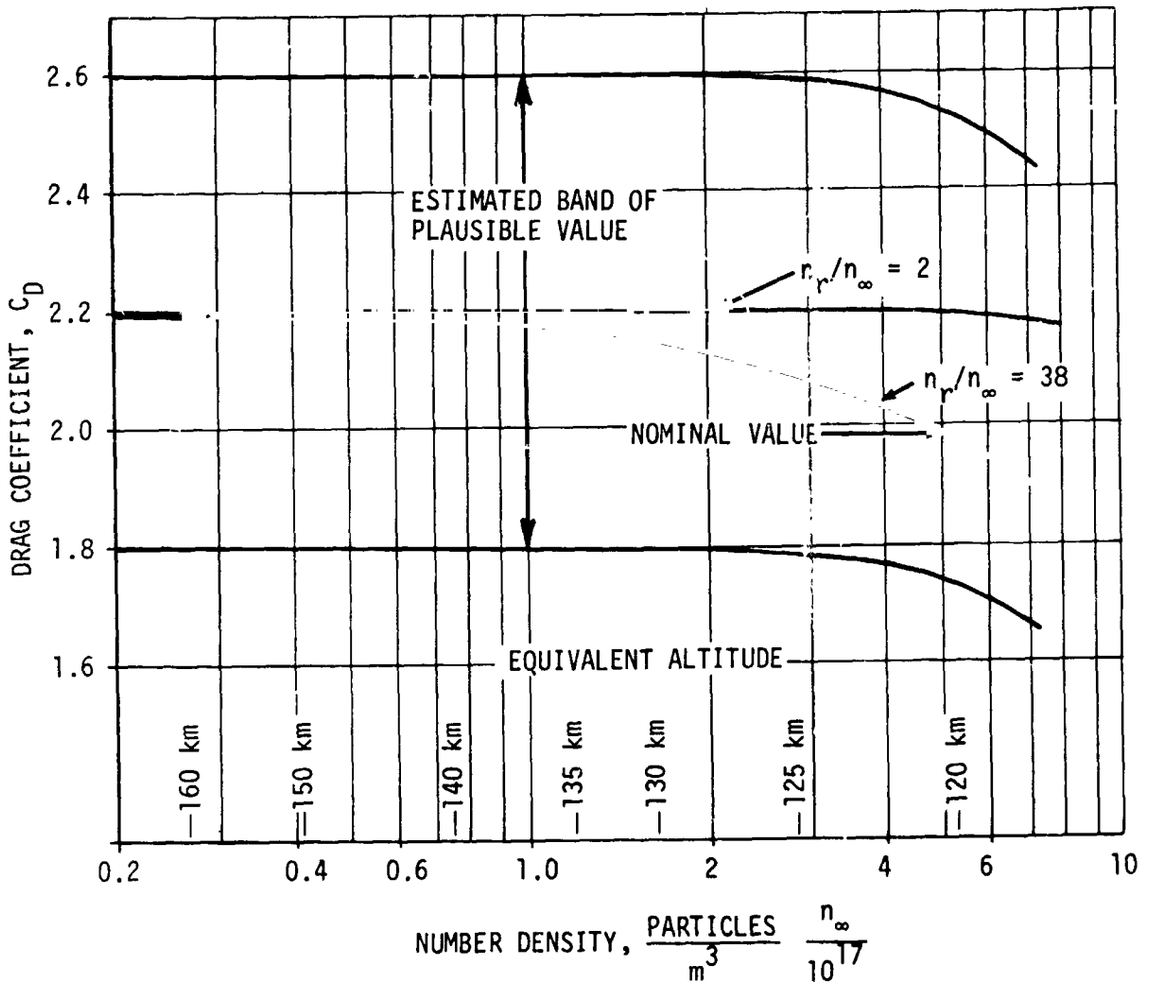

Figure 2-9. RANGE OF DRAG COEFFICIENTS VS ALTITUDE FOR 0.7 M DIAMETER SPHERICAL SATELLITE (REF. 26)

$$C_{D_I} = 2(1 + S^{-2}) \tag{1}$$

where S is the speed ratio and is assumed greater than five for this case. The remainder of the satellite drag, excepting electric, magnetic, and radiation pressure effects, is due to the recoil momentum of reflecting molecules from the satellite's surface leading to a coefficient of drag that may be denoted as C_{D_R}. This requires knowledge of the reemitted molecular velocity distribution. This velocity distribution is unknown but numerous models are available such as those by Nocilla (1961, ref. 27 and 1963, ref. 28) and Schamberg (1959, ref. 29). All model studies show considerable variation; however, for a spherical satellite near perigee of the drag-free orbits proposed by Cannon (see Cannon, et al., 1966, ref. 26 and Walters, et al., 1968, ref. 30), C_{D_R} falls in the range $-0.5 \leq C_{D_R} \leq 0.9$. The nominal value $C_D = C_{D_I} + C_{D_R} = 2.2$ falls in the middle of this range. Thus, the true C_D most likely lies in the range of $1.8 \leq C_D \leq 2.6$. Experimental studies in laboratories and with earth satellites tend to verify this C_D range.

Drag coefficients higher than 3.0 are believed impossible in spite of a value of 4.4 calculated from Explorer XVII data (Cannon, et al., 1966, ref. 26). Mechanisms which can lead to a high C_D are:

- Preferential reemission in the exact upstream direction with no energy absorption from the incident molecules by the satellite surface. However, no analytical or experimental evidence of this possibility exists.
- Conversion of potential energy of dissociated oxygen to kinetic energy of reemitted O_2 molecules. This effect is considered unlikely because the recombination energy would be mostly absorbed by the satellite rather than appearing as kinetic energy of the reemitted oxygen molecule.

Two important conclusions were derived by Moe from a study of the Explorer VI paddlewheel satellite (Moe, 1966a, ref. 31). The first is that the relevant surface of the satellite, whether a layer of adsorbed gas or a clean, solid substrate, reached steady state within a short period of time. This conclusion

is considered valid because the drag coefficients, as indicated by combined ephemeris and spin decay measurements, did not change by more than one percent from the first day until the tenth. The second is that significant drag effects caused by surface recombination of atomic oxygen or dissociation of molecular nitrogen at 270 km, were very unlikely.

Section III

THE ODYSSEY I EXPERIMENTS

The ODYSSEY I experiment program is designed to determine the drag coefficient of earth orbiting satellites, the nature of the gas-surface interaction phenomena, the distribution of the incident and reemitted molecular flux, and the density variation of the upper atmosphere. The ODYSSEY I experiment package includes: a paddlewheel/diffuse sphere combination, a gas-surface interaction experiment, a mass spectrometer package, and the passive sphere ensemble. The possibility of placing additional experiments onboard the ODYSSEY package has been considered. Although they are not presented as an integral part of the ODYSSEY package, a thermal probe experiment and an EUV (extreme ultraviolet) and/or an X-ray extinction experiment were considered as possible additions. Again, if payload volume, power, and electronics are available, one or both of these additional experiences could be added to the ODYSSEY package.

The specific mission objectives may be listed as follows:

- Determine satellite drag coefficients in situ in a free-molecular-flow regime.
- Establish accommodation coefficients for engineering surfaces at orbital speeds and energies.
- Investigate the gas-surface interaction phenomena in situ in the 130 to 240 km altitude range through a detailed study of the velocity distributions of the incident and reflected gas beams.
- Improve the present capability for predicting satellite lifetime in near-earth orbits and improve the design of attitude control systems by improving aerodynamic torque predictions.
- Determine the incident molecular flux and absolute mass density.
- Substantiate or improve existing model atmospheres for density and composition at altitudes between 130 and 240 km, and compare various density measuring techniques.
- Provide data that will aid in giving a more consistent picture of the entire thermosphere.
- Establish the drag coefficient for spherical satellites in the free- and near-free-molecular-flow regime around 160 km.

- Establish more precisely the exact geodetic station locations and higher order earth gravitational harmonics terms.

3.1 PASSIVE DRAG SPHERES

The Passive Drag Spheres ensemble has been proposed by Dr. C. A. Lundquist and associates of the Smithsonian Astrophysics Observatory (SAO) as a means of determining atmospheric density and drag coefficients in the free- and near-free-molecular-flow regime, 1967, (ref. 32). Specifically, it has been suggested that these spheres be orbited with a nominal perigee of 150 km and an apogee of 2000 to 4000 km. As discussed previously, the amount of data regarding atmospheric densities and the near-free-molecular-flow effects on satellite orbital lifetimes is deficient for altitudes below about 240 km. With the advent of the highly accurate tracking capability of the Baker-Nunn cameras, optical tracking of orbital satellites has become routine for the SAO tracking network. Thus, an experiment has been designed that will allow atmospheric density and drag coefficients to be determined from the observed orbital dynamics of the experiment package.

The suggested experiment consists of orbiting three spheres having equal area/mass ratios and a fourth sphere having the same diameter as one of the other three, but having a much higher density. The diameters of the first three spheres are proposed to be 0.7 m, 0.4 m, and 0.3 m. The high density sphere will have a diameter of 0.4 m and is specifically designed to provide additional data regarding geodetic station location, higher order earth gravitational harmonics terms, and temporal variations of the atmosphere. All four spheres will be constructed of the same material and will have the same surface finish.

3.1.1 Aerodynamic Drag Coefficient

A representation of the aerodynamic drag coefficient with which to correlate subsequent data must be adopted for this experiment. Unfortunately, a large number of formulas are available having been suggested by different workers using experimental approaches. A recent comparison of experimental results with the most widely accepted theoretical expressions for the near-free-molecular-flow drag coefficient has been presented by Maslach, et al.,

1964 (ref. 33). An excellent discussion of the practical aspects of drag coefficients of spherical satellites has been written by Cook, 1966 (ref. 34). Most of the investigators agree on the form of the drag coefficient equation; however, complete agreement has not been reached on the values to be assigned to the terms relevant to the interaction model and the satellite geometry. A discussion of some of the theoretical methods for predicting near-free-molecular-flow drag coefficients is given in Appendix A.

3.1.2 Experiment Concept

The orbital lifetime of the four passive spheres depends, in a complex manner, on the accommodation coefficient and the gas-surface interaction. These effects are lumped into the value of the drag coefficient which is to be determined. The three spherical satellites (introduced earlier) having the same area/mass ratio (A/m) will be designed to have uniform and near-equal surface temperatures and will be launched by a single vehicle into the same initial orbit. The rate of change of the period of any of the three spheres may be written as (Sterne, 1958, ref. 35):

$$\frac{dP}{dt} = -\frac{3}{2}\frac{A}{m}\rho_p\, a \int_o^{2\pi} C_D \frac{\rho}{\rho_p}\frac{(1 + e\cos E)^{3/2}}{(1 - e\cos E)^{1/2}}\, dE \qquad (2)$$

The derivation of equation (2) is given in Appendix B. If the quantities f_1 and f_2 are defined as

$$f_1 = \int_o^{\pi} \frac{\rho}{\rho_p}\frac{(1 + e\cos E)^{3/2}}{(1 - e\cos E)^{1/2}}\, dE \qquad (3)$$

$$f_2 = \int_o^{\pi} \left(\frac{\rho}{\rho_p}\right)^2 \frac{(1 + e\cos E)^{3/2}}{(1 - e\cos E)^{1/2}}\, dE \qquad (4)$$

then equation (2) may be written as

$$\frac{dP}{dt} = -3\, a\, f_1 \frac{A}{m} C_{D_{fm}} \rho_p + 3\, a\, f_2\, B \frac{A}{m} D\, F\, \rho_p^2 \qquad (5)$$

where C_D has been replaced with the form of equation (A-1) given in Appendix A. Tables for f_1 have been formulated by Jacchia and Slowey, 1963 (ref. 36), and similar tables may be constructed for f_2.

Any two of the three satellites will now give two linear equations for the two unknown quantities $C_{D_{fm}}\rho_p$ and $BF\,\rho_p^2$ from equation (5). As discussed previously, all other values in the equation are assumed to be known or can be determined from the orbital parameters. By assuming the value of $C_{D_{fm}}$ from equation (A-5) to be correct (or by taking a value from some other source, i.e., Cook, 1965, (ref. 12)) ρ_p may be obtained from the product $C_{D_{fm}}\,\rho_p$. This value of ρ_p can be used to obtain BF from the product of $BF\rho_p^2$. If the value B is assumed to be known, then F and C_D may be immediately obtained from equation (A-1).

The discussion in the foregoing paragraphs has been oversimplified, hopefully illustrating the principal features of the analysis. The use of the third sphere provides substantiation of the results of the other two spheres. However, corrections remain to be made for many of the preliminary assumptions. For example, corrections must be made as the satellites separate farther and farther apart, scale height corrections must be made to ρ_p, and corrections must be made for the effects of higher-order harmonics in the gravitational field. Most of the effects are second-order effects and the corrections may be small. If necessary, the terms which were neglected in the equation for da/dE may be reinstated and the equations for de/dE and di/dE may be employed to provide higher order corrections (See Appendix B).

Lundquist, 1967, (ref. 32) states that a useful lifetime of three to four months would be sufficient for the passive spheres. The useful lifetime is impaired as the spheres separate farther and farther apart, and depends in part on the apogee radius which will probably be the maximum distance the Baker-Nunn network can track (tracking is done at apogee). This distance will be between 2000 and 4000 km. However, three to four months of useful lifetime can be readily obtained. The dense sphere will have a useful lifetime of at least a year. The area to mass ratios will be determined by Lundquist and associates.

3.1.3 The Geodetic Sphere

The fourth sphere, the geodetic sphere, will be inserted into orbit along with the other three. This sphere will have a diameter of 0.4 m and a much higher density than any of the other spheres. The orbital lifetime of this high-density sphere will be longer than any of the other three due to its higher density. From a knowledge of the drag coefficient derived from the other spheres, this sphere will provide additional data relevant to the temporal variation of the atmospheric density due to solar and geophysical events. However, the main function of the geodetic sphere is the determination of the higher-order terms in the expansion of the earth's gravitational potential and establishment of exact tracking station locations.

3.2 PADDLEWHEEL/DIFFUSE SPHERE EXPERIMENT

Orbiting a paddlewheel or spin satellite along with a diffusely reflecting, fully accommodating (honeycomb) sphere has been proposed by Dr. O. K. Moe (ref. 37). The experiment objective is to determine satellite drag coefficients, the nature of molecular gas-surface interactions, and absolute atmospheric densities in a free-molecular-flow regime.

Paddlewheel satellites such as Explorer VI and Ariel II have been employed to determine drag coefficients and atmospheric densities from spin-rate data. Also, spin and orbital decay rates of these satellites were used with gas-surface interaction models to calculate satellite drag coefficients and accommodation coefficients (Moe, ref. 31 and ref. 38). Orbital energy levels and orbital contamination levels were, therefore, simulated on engineering surfaces, a condition which is not attainable in current laboratory experiments.

The proposed paddlewheel satellite would orbit the earth with a nominal 200 km initial perigee and a 2000 - 4000 km apogee. The diffuse sphere would be in an identical orbit. The honeycomb or diffuse sphere is to be designed to be a nearly perfect diffusely reflecting, fully accommodating body. Thus, the drag coefficient of the diffuse sphere can be obtained since the nature of the gas-surface interaction for diffusely reflecting, fully accommodating

bodies in a free-molecular-flow regime is relatively well defined. Then the same technique as was used in calculating density from observation of orbital decay for the passive drag spheres can be employed. Thus, application of Sterne's general equation where the orbital parameters are determined by tracking of the satellite's orbit provides a measure of the absolute density at altitude.

A significant improvement to the ODYSSEY I experiment package could be accomplished by placing both the passive sphere ensemble and the paddlewheel/diffuse sphere combination into the same orbit. Both experiments would then directly complement each other. For example, the free-molecular-flow drag coefficients determined by the paddlewheel can be compared with, and used to verify the $C_{D_{fm}}$ computed from equation (A-5). This would allow a more accurate determination of the near-free-molecular-flow drag coefficient. Also, since all theoretical models for predicting near-free-molecular-flow drag coefficients are based on fully accommodating, diffusely reflecting models, the diffuse sphere would provide such an in situ model to compare with various theoretical models. The density values derived from the passive spheres should also provide an interesting comparison with the density values deduced from the diffuse sphere.

The paddlewheel satellite must have a spherical central body diameter of approximately 12 inches to house the required electronics. As a more favorable alternate, an 8 inch diameter hemispherical central body with trailing cone, having a 7 inch base diameter with a 36 inch altitude could be employed as shown on the following page. Tentatively, the paddlewheel satellite will be about 40 inches tip-to-tip and will house a battery, battery charge unit, a DC-DC converter, A/D converter, multiplexer, transponder, receiver, transmitter, subcarrier, the sun sensor electronics, signal conditioner, sun sensor, rotary solenoid, rotary potentiometer, nutation damper, and a tape recorder. The central body must be large enough to house the necessary electronics but small enough so that the paddles constitute the primary drag area and can effectively spin the satellite up or down. Also, care must be taken to avoid collisions with the paddles by a molecule which first hit the central body or vice versa.

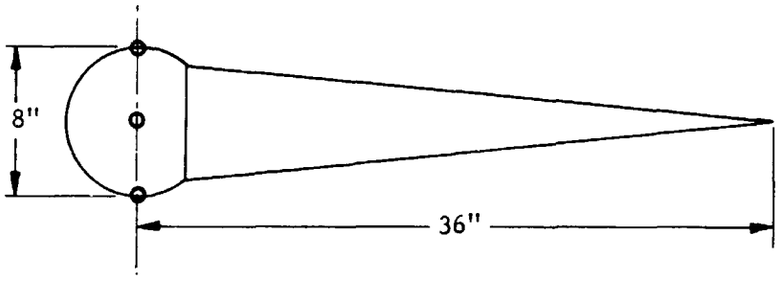

NOTE: FOUR PADDLES WILL BE SYMMETRICALLY MOUNTED ON THE HEMISPHERE PORTION OF THE PADDLEWHEEL SATELLITE AS INDICATED BY THE DOTS (o) SHOWN IN THE ABOVE SKETCH.

The hemisphere-cone configuration should be able to house the necessary electronics and prevent secondary collisions from exceeding two percent of the reflected molecules. The hemisphere would face the free-stream flow.

The size allotment permits an 8" diameter hemisphere, four 8" long support rods, and four 8" x 8" paddles. Tentatively, these sizing figures and the requirement that the paddlewheel be in a free-molecular flow regime, places the minimum perigee altitude at 180 to 200 km. However, the paddlewheel dimensions are merely nominal values. They can be decreased enabling the paddlewheel/diffuse sphere combination to have the same perigee altitude as the passive sphere ensemble, namely 150 to 180 km.

Orbital tracking measurements of the paddlewheel satellite, probably by the Baker-Nunn optical tracking stations and the STADAN network, would determine orbital decay rates. The spin decay is assumed to be almost entirely

caused by the momentum of the reemitted molecules while most of the orbital decay is caused by the incident molecular momentum. The drag and accommodation coefficients could then be calculated from Schamberg's gas-surface interaction model or similar models. Schamberg's accommodation model is described in Appendix C.

3.2.1 Calculation Procedure

The values proposed to be determined from this experiment are: satellite drag coefficients; the accommodation coefficient, α; and absolute atmospheric density. The angular distribution can be taken from Schamberg's model. The dependence of the accommodation coefficient on satellite substrate material and on angle of incidence has been assumed to be negligible. However, the paddle angles will be varied to check the influence of the angle of incidence on C_D and α.

Once the spin decay rates, orbital decay rates, paddle temperatures, and the other orbital parameters have been determined, the torque, $\bar{\tau}$, about the spin axis averaged over a spin cycle would be calculated from

$$\bar{\tau} = G\,\rho V_i^2 \tag{6}$$

where V_i is the instantaneous satellite speed relative to the atmosphere and G is given as

$$G = -4LJA\left(K_1\frac{V_r}{V_i} + K_2\right). \tag{7}$$

Here, L is the perpendicular distance from a paddle center to the spin axis, A is the area of one side of a paddle, and J is given as

$$J = \left(1 - \frac{\cos^2\xi}{\cos^2\theta'}\right)^{1/2} \tag{8}$$

where the angles ξ and θ' depend on the paddlewheel geometry and are defined by Moe, (ref. 31). The functions K_1 and K_2 depend on the gas-solid surface interaction model.

By equating the spin angular momentum change in one orbital revolution to the corresponding time integral of the average torque, $\bar{\tau}$, a relationship may be obtained between the following parameters: G; the observed spin-rate change; and ρ_p, the atmospheric density at perigee. The density is known from the diffuse sphere satellite or can be eliminated by its relationship with the change in semimajor axis, Δa, and the drag coefficient, C_D (King-Hele, 1964, ref. 39).

The resulting expression for G becomes

$$G = - \frac{C_D P_o I_r A (1 + e)}{m(1 - e^2)^{1/2}} \frac{\Delta\nu}{\Delta a} \tag{9}$$

where

P_o = period of orbital motion

I_r = satellite's roll moment of inertia

A = satellite effective drag area

m = satellite's mass

e = orbital eccentricity

$\Delta\nu$ = spin-rate change per revolution

Δa = semimajor axis change per revolution.

By equating the above two expressions for G and employing Schamberg's equation for C_D to eliminate V_r, an expression is obtained relating C_D to the observed changes in spin-rate and semimajor axis; namely,

$$C_D = \frac{2\left(1 - \frac{K_2 K_3}{K_1}\right)}{1 - \frac{2K_3 P_o I_r A (1 + e)}{K_1 m(1 - e^2)^{1/2}} \frac{\Delta\nu}{\Delta a}} \tag{10}$$

where K_1, K_2, and K_3 are functions of the body geometry and the nature of the gas-surface interaction. Models developed by Schamberg or other investigators (Alcalay and Knuth, 1966, ref. 40; Maxwell, 1890, ref. 41, Nocilla, 1963, ref. 28; etc.) can be applied in an effort to see what models best describe the

actual interaction. Because the energy accommodation coefficient, α, may be given as

$$\alpha = \frac{1 - \left(\frac{V_r}{V_i}\right)^2}{(T_i - T_w)/T_i} \simeq 1 - \left(\frac{V_r}{V_i}\right)^2 \tag{11}$$

then α may be shown to be

$$\alpha = 1 - \left(\frac{C_D - 2}{2K_3}\right)^2 \tag{12}$$

Values of α computed for the paddlewheel at varying angles of incidence should yield typical values of α for satellite surfaces and indicate whether it varies with angle of incidence. If α varies with angle of incidence in a systematic manner, more general equations must be formulated to describe the gas-surface interactions. In the preceding drag calculations, the reference drag area was taken as the projected area normal to the incident velocity vector.

3.2.2 Secondary Effects

Once the drag and accommodation coefficients and the atmospheric density have been determined, density comparisons can be made with model atmospheres. Analytical and experimental drag and accommodation coefficient models can also be used for comparison. Moe, (ref. 31) determined the drag coefficient on the paddlewheel satellite Explorer VI to be 2.50 ± 0.06 and the accommodation coefficient to be 0.65 ± 0.09 using Schamberg's model with a diffuse distribution of reemitted particles. Moe concluded that recombination, dissociation, sputtering, and errors due to a non-Maxwellian distribution of molecular speeds were negligible. Placing the passive sphere ensemble into the same orbit as the paddlewheel/diffuse sphere combination, allows an investigation to be made of the effect of the satellite surface on the drag coefficient. For example, the drag coefficient values deduced by the diffuse sphere can be compared with the drag coefficients on the "smooth" passive, engineering surface spheres. Possibly, additional spheres made of stainless steel, aluminum, gold, glass, tungsten, or another "special" type of surface could be added to the package. From the knowledge of the atmospheric density determined from the orbital decay

of the diffuse sphere, the additional spheres should reveal information pertinent to the effect of surface material and absorbed gas layers on the drag and accommodation coefficient.

3.3 GAS-SURFACE INTERACTION EXPERIMENT

An experiment designed to obtain useful and quantitative measurements of gas-surface interactions at satellite energy conditions in situ has been proposed by Dr. Jens C. Zorn of the Randall Laboratory of Physics, University of Michigan (ref. 42). This experiment will provide information on gas-surface momentum and energy transfer through a detailed study of the velocity distributions of the incident and reflected gas beams. The flux of the reflected particles, and an analysis of the composition, velocity distribution, and angular distribution of the reflected stream will be determined. A metastable detector will be employed for measurements of the velocity distributions and a mass spectrometer will be employed for the measurement of flux composition. A quadrupole mass spectrometer will measure the composition of the incoming flux. The flux of N_2 alone will also be measured.

The experiment concept will involve the investigation of the interactions of the incident N_2 molecules with engineering and scientific surfaces under satellite energy and environment conditions. The composition of the total molecular flux incident on the satellite is measured. Also the angular distribution of the N_2 molecules which are scattered from the target surface will be measured.

The altitude range of this experiment can be from 100 to 350 km. The lower limit (100 km) results from mean free path considerations: free-molecular-flow cannot be achieved below this altitude. The upper altitude limit is reached when the N_2 flux becomes too weak to be measured. The perigee altitude used for this experiment on the ODYSSEY experiment package will be 160 to 180 km.

Figure 3-1 shows a general view of the proposed gas-surface interaction experiment. The quadrupole mass spectrometer which measures the composition of the incoming flux, is shown on one side. A time of flight (TOF) N_2 analyzer is shown on the other side. In between these two instruments is an analyzer

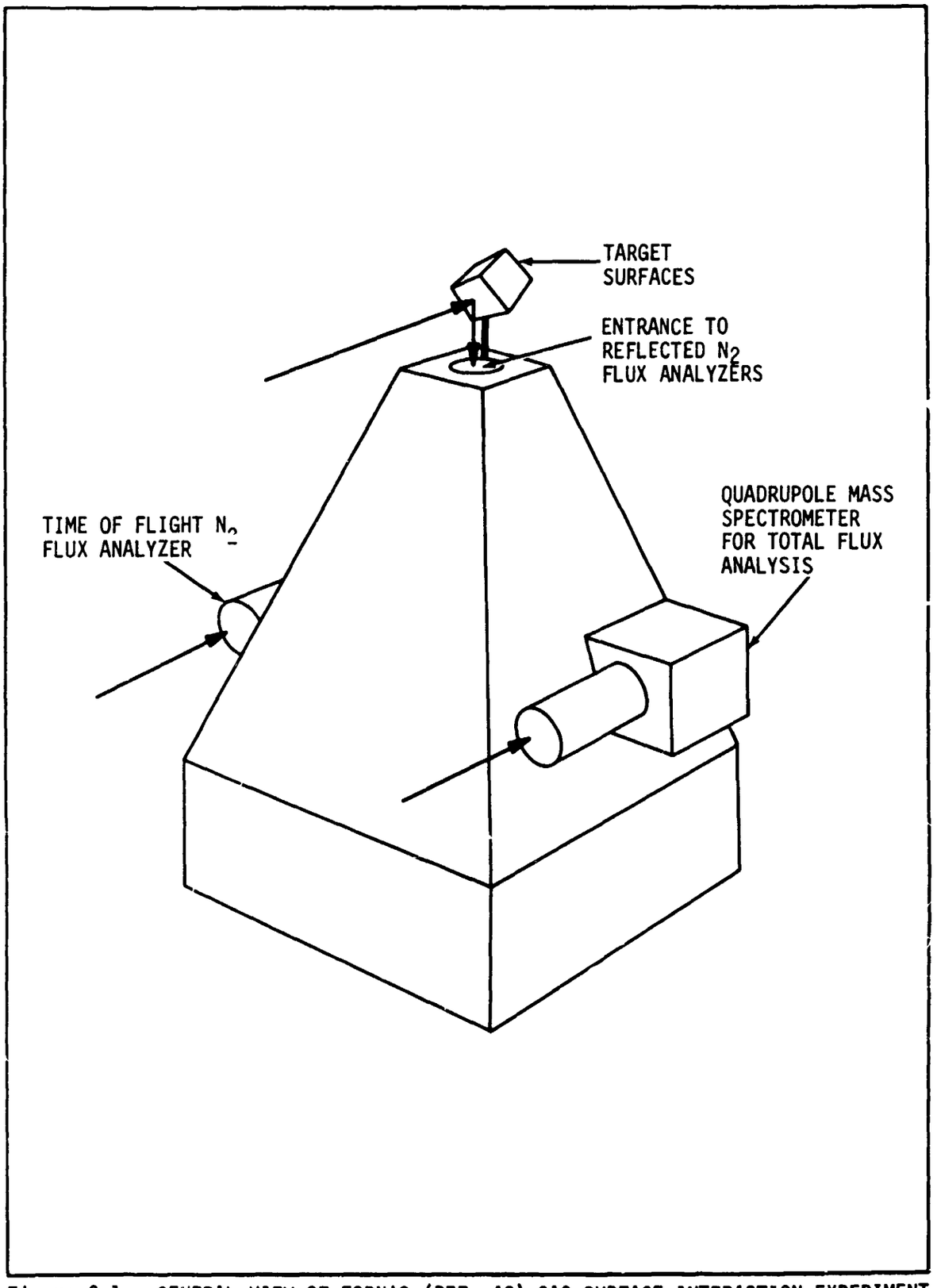

Figure 3-1. GENERAL VIEW OF ZORN'S (REF. 42) GAS-SURFACE INTERACTION EXPERIMENT

used for the measurement of the angular and velocity distribution of the N_2 flux which is reflected from the target surface. Molecules will strike the target surface at various angles depending on the spacecraft's orientation with respect to the velocity vector. Attitude stabilization is not required, therefore the tumbling of the vehicle provides a variety of incidence angles for the molecu es on the target.

The velocity distribution of the reflected flux is analyzed by a metastable time of flight (MTOF) analyzer. Basically, a pulsed electron gun is used to create a spatially concentrated group of neutral metastable N_2 molecules. The time of flight of these metastables over a 20 cm path within the apparatus will be observed. Since the metastable molecules are neutral, the detector output will provide a measure of the velocity distribution of the reflected neutral flux.

3.3.1 Description of the TOF Analyzer

The molecules enter the N_2 TOF analyzer directly for flux measurements, or indirectly after first colliding with a target surface. In either case, the molecules then pass through a pulsed electron gun where some of them are excited to their metastable state. If a metastable molecule passes through the collimator, or array of parallel tubes, without a collision, it will arrive in its excited state at the metal detector surface. At the metal detector surface the metastable molecule undergoes a radiationless decay (or a so-called "Auger Process") and ejects an electron from the metal. These electrons are then accelerated into a multiplier, the output of which becomes a series of pulses at a rate proportional to the flux of metastable molecules through the analyzer. Appendix D provides a basic discussion of metastable states and the Auger Process.

Figure 3-2 describes the N_2 TOF analyzer operation and the measurement of the angular dis: ɔution of the reflected flux. This figure as well as the entire discussion of this experiment was taken from Zorn, 1967 (ref. 42). The reader is referred to reference 42 for details of this experime t. The author discusses methods of alleviating background noise signals due to ions, photons, and background molecules.

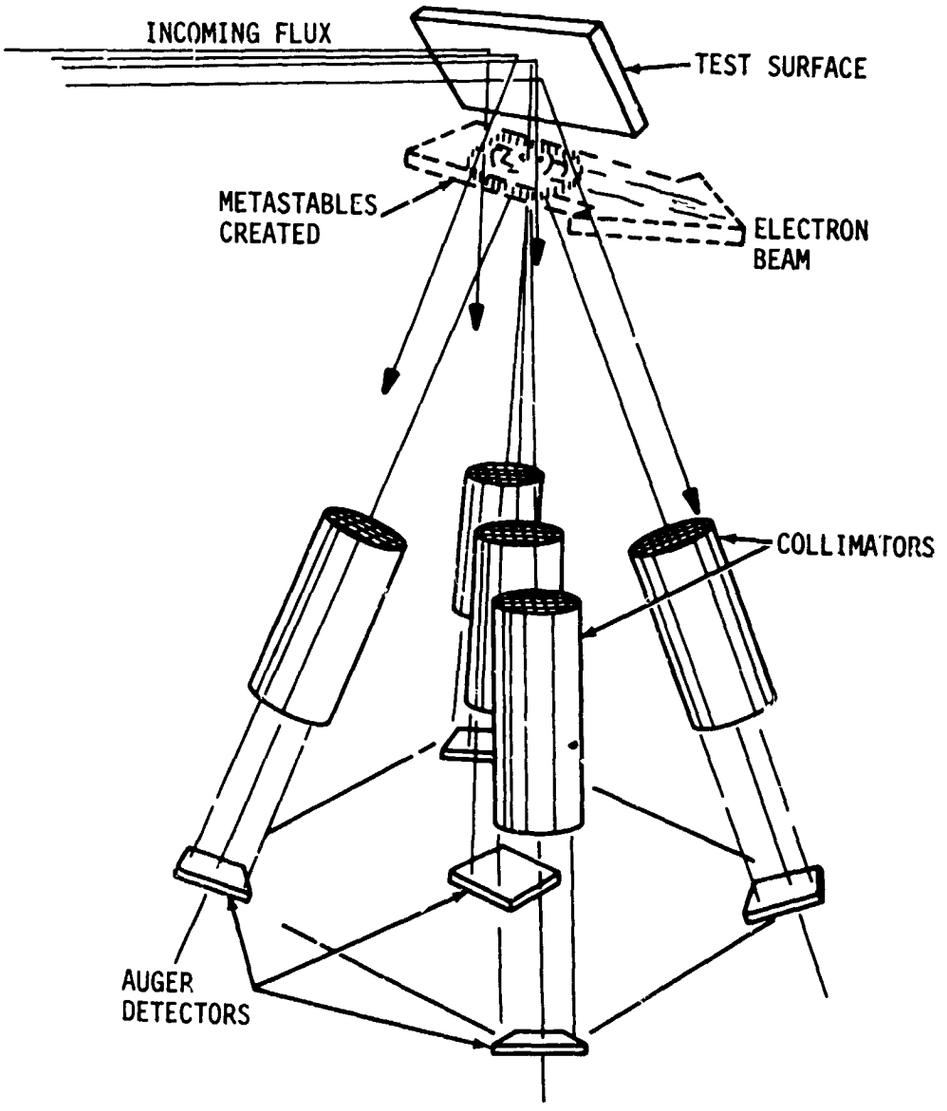

Figure 3-2. MEASUREMENT OF ANGULAR DISTRIBUTION OF THE REFLECTED FLUX, ZORN, REFERENCE 42

In the same reference, the author provides a detailed discussion of the TOF velocity distribution analysis, the properties of N_2 in relation to TOF analysis, Auger detector surfaces for metastable molecules, and the test surfaces employed for the gas-surface interaction study.

The analysis of the velocity and angular distribution as well as some of the experiment details are discussed in Appendix E. The assumptions made in Appendix E were investigated by Zorn (ref. 42). For the most part, it was determined that these assumptions were not always justified but that generally the resulting effects were small and could be accounted for.

In addition, consideration is given to the relationship of collisions to the velocity distribution. Since the molecules in the reflected beam must pass through a background gas during the measurements, the collisions between molecules of the beam and those of the background gas must not introduce any error into the velocity distribution measurements. Here two points are of special merit:

(1) When good angular resolution is wanted in the analysis of the reflected beam, even small angle collisions are important. The usual experimental verifications of mean-free-path calculations are not sensitive to the occurrence of glancing encounters between molecules.

(2) Long range interactions between molecules may not involve enough momentum transfer to qualify as a collision in the gas kinetic sense, but such an interaction may quench a metastable molecule and thus remove it completely from the detectable component of the reflected beam.

Regarding the points made in the above paragraph, Zorn (ref. 42) derived a modification of the velocity distribution by collisions and evaluated its effects. Zorn also considered the importance of residual gas scattering in gas-surface interaction experiments. Basically, since the molecules in the reflected beam must pass through a background gas during the measurements, one must insure that collisions between molecules of the beam and those of the background gas will not introduce systematic errors into the results of the velocity distribution measurements. If sufficient background gas is present the detected flux may well be deficient in slow molecules. Since accommodation at

a surface is judged by comparing the incoming velocity distribution (dominated by the satellite velocity) with the distribution measured in the reflected beam, accommodation may be underestimated if the effects of residual gas scattering are ignored.

Finally, an efficient Auger detector surface is to be selected. An efficient Auger surface is one through which electrons can easily tunnel. The choice of detector surfaces for metastable states above 10 ev (above ground state) is not critical. For systems of a lower metastable energy (e.g., 0_2) it is desirable to use a low work function metal for the detector surface. Also contamination of the detector must be avoided in some cases. For an N_2 beam, a tungsten plate serves as an effective detector surface. However certain unclean or contaminated surfaces also function equally well in this case.

The target surfaces considered for this experiment will be typical engineering materials such as stainless steel, aluminum, titanium, and solar cell units. Also a special scientific surface for calibration purposes will be employed. This surface will be a vapor-deposited surface or a calibration surface prepared by crystal cleaving.

3.4 MASS SPECTROMETER PACKAGE

To complement the density measurements determined by the orbital tracking of the paddlewheel/diffuse sphere and passive sphere ensemble and the quadrupole mass spectrometer on the GSI (Zorn, ref. 42) experiment, two or three additional mass spectrometers will be employed. Tentatively, one or two quadrupole mass spectrometers of the type proposed by Dr. Richard J. Leite (ref. 43) may be used. Another alternative would be to fly three magnetic deflection mass spectrometers of the type proposed by Nier (Kasprzak, 1968, ref. 2, or Krankowsky, 1968, ref. 3). In this case it would be advantageous to fly one open ion source and two closed ion source spectrometers. Comparison between the open and closed ion source spectrometers would provide a quantitative measure of the 0 concentration.

The primary objective of any mass spectrometer package would be to measure the concentrations of N_2, 0_2 and 0. In addition, measurements of additional

constituents between 0 and 50 Atomic Mass Units would be useful in order to derive a total absolute density as a function of time in orbit and perigee altitude.

The principle of operation of all mass spectrometers may be described briefly as follows: a sample of gas is introduced into a region where ionization takes place. That portion of the sample which becomes ionized is acted upon by electrostatic and/or magnetic fields. The separate components are collected and detected as current, usually of the order of microamps. Further details on the operation of mass spectrometers can be found in a report entitled "Introduction to Mass Spectrometers" written by SDS Aerospace Systems, 1966 (ref. 44).

The reported accuracy of mass spectrometers is discussed by Leite (ref. 42), Krankowsky (ref. 3), Kasprzak (ref. 2), or Von Zahn (ref. 1). The greatest uncertainty involves the qualitative determination of the abundance of O. There is no satisfactory method available for making a direct calibration of flight mass spectrometers for atomic oxygen (Hedin and Nier, 1966, ref. 19). In view of this, the best value of atomic oxygen number densities that can be measured is estimated to be no better than approximately 20 to 25 percent.

3.5 POSSIBLE ADDITIONAL EXPERIMENTS

In addition to the basic ODYSSEY package consisting of the paddlewheel/diffuse sphere, passive sphere ensemble, the GSI experiment, and the mass spectrometer package, three additional experiments could possibly be added to the ODYSSEY package. These experiments consist of an Aerospace Corporation EUV extinction experiment, the Coordinated Science Laboratory gas-surface interaction experiment, and a Faraday Laboratory gas-surface interaction experiment. These three experiments are described in the next section of this report.

The reason for considering possible additions to the ODYSSEY experiment originates from the fact that extra power and volume may be available from the experiment carrier. That is, a carrier vehicle, possibly the Small Standard Satellite (S^3), or something similar, will be used to house the University of Michigan GSI experiment and the mass spectrometer package. Thus, the carrier

vehicle selected for this purpose could easily be large enough and have enough additional power to encompass either the EUV extinction experiment, or the Faraday Laboratory GSI experiment, or both. The Coordinated Science Laboratory (CSL) GSI experiment could possibly be included with the paddlewheel/diffuse sphere and passive sphere ensemble in the same launch vehicle payload compartment.

The paddlewheel/diffuse sphere, passive sphere ensemble, possibly the CSL-GSI experiment, and a carrier designed to house the University of Michigan GSI experiment, the mass spectrometer package, and possibly the EUV extinction experiment, and Faraday Laboratory GSI experiment will all be packaged into some launch vehicle payload compartment. One or two launches may be required to place all the experiments into the required orbit. All experiments will be in the same orbit (150 to 180 km x 2000-4000 km). An Engineering Implementation Plan, to be published this year, will describe the experiment carrier and method of launch.

Section IV

COMPARISON OF ODYSSEY I AND OTHER EXPERIMENTS HAVING SIMILAR GOALS

A large number of other experiments having goals similar to those of the ODYSSEY I experiment have been reviewed (Walters, et al., 1968, ref. 30). Some of these experiments have already been launched while others have only been proposed. The experiments presented here may be considered representative of the many different types of investigations. Only the most significant of all the experiments were selected for comparison with the ODYSSEY I experiment package.

This section updates the discussion presented in Section IV of reference 30. Thus, many of the experiments described in reference 30 are not repeated here. Instead, some of the more recent experiments related to the ODYSSEY package are either discussed for the first time or updated and expounded upon from their discussion in reference 30. The reader is referred to reference 30 for a discussion of other experiments relevant to ODYSSEY.

4.1 MEASUREMENTS OF ATMOSPHERIC COMPOSITION

4.1.1 Aerobee Rocket and Solar Extreme Ultraviolet Measurement Flights

Two Aerobee rocket flights (NC 3.115F and NASA 4.127 UA) were launched from White Sands, New Mexico on 0730 MST June 6, 1963, and 0345 MST April 15, 1965, respectively. These flights are discussed by Nier, et al., 1964 (ref. 45), Hedin and Nier, 1966 (ref. 19), Hedin and Nier, 1965 (ref. 46), and Hedin, et al., 1964 (ref. 47). Reference 30 discusses the mass spectrometer data from the references listed above.

Also, Hall, et al., 1965 (ref. 20) obtained number densities from solar extreme ultraviolet (EUV) absorption measurements employing a rocket borne telemetering grazing incidence monochromator. This method makes use of the atmospheric absorption characteristics for solar EUV radiation (Hinteregger, ref. 48 and 49; Hall, et al., ref. 50). Figures 4-1, 4-2, and 4-3 indicate the results of this test performed over White Sands, New Mexico on 10 July 1963,

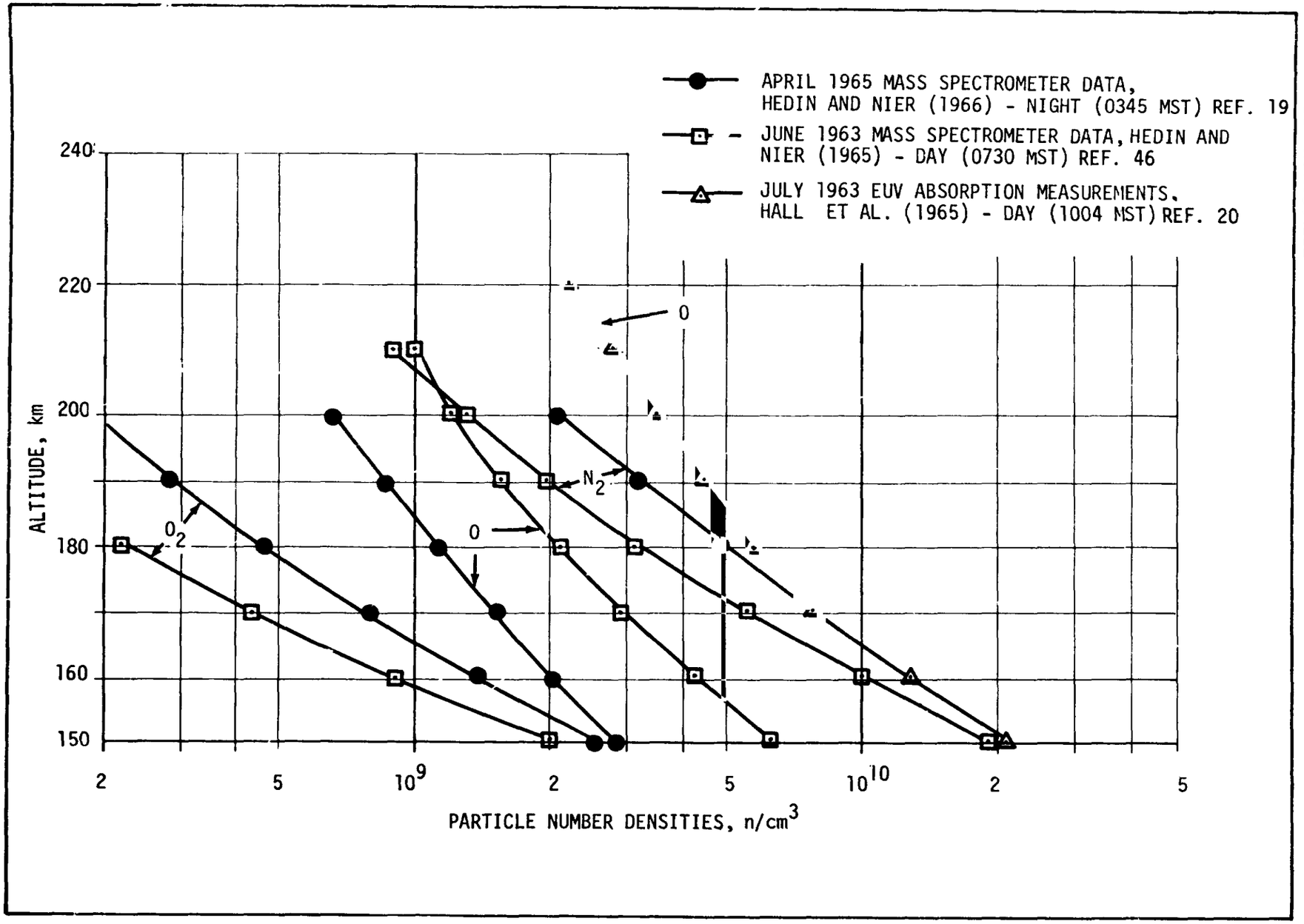

Figure 4-1. SELECTED PARTICLE NUMBER DENSITIES OF THE UPPER ATMOSPHERE FROM 150-220 KM

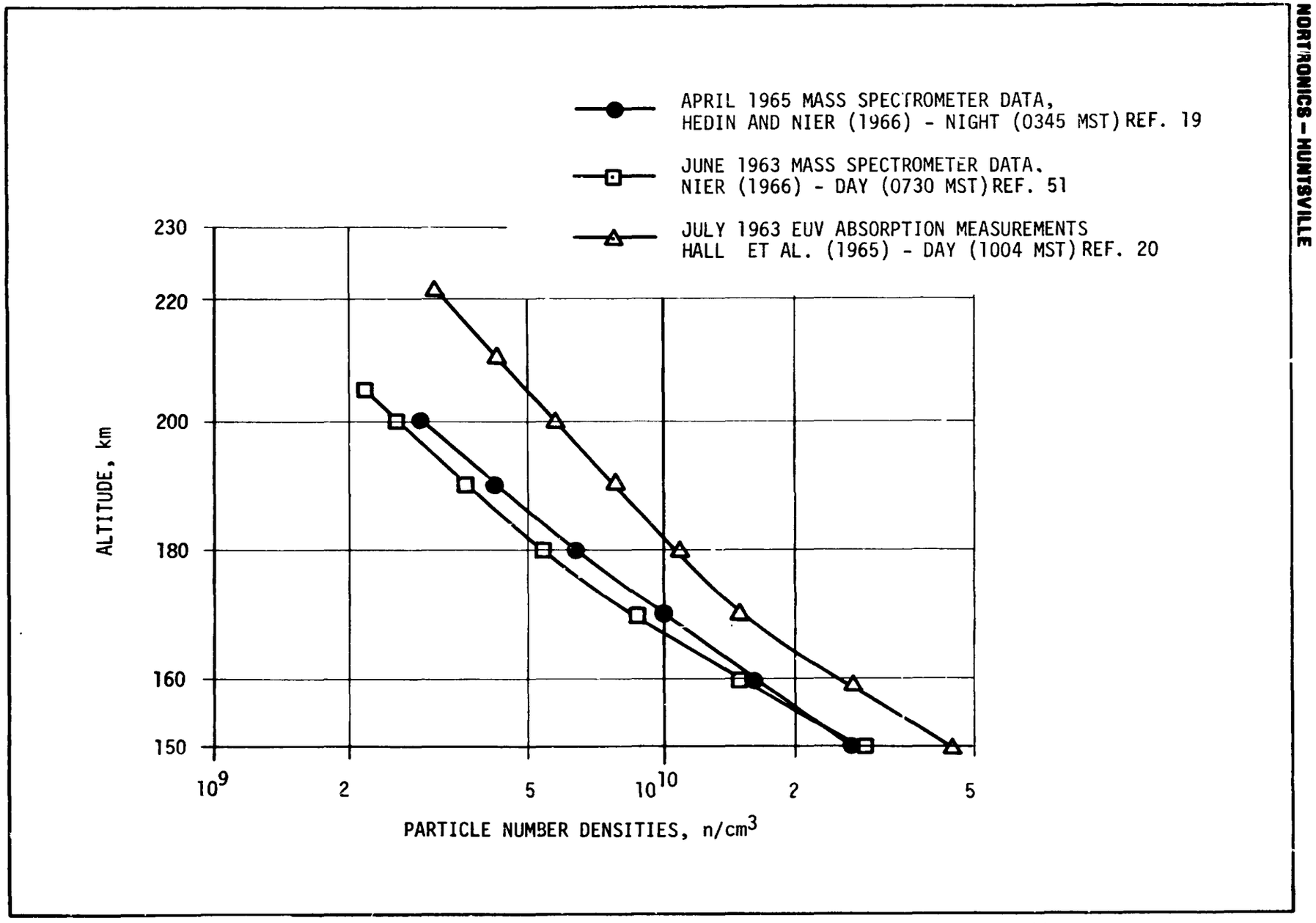

Figure 4-2. TOTAL PARTICLE NUMBER DENSITIES OF THE UPPER ATMOSPHERE FROM 150-220 KM

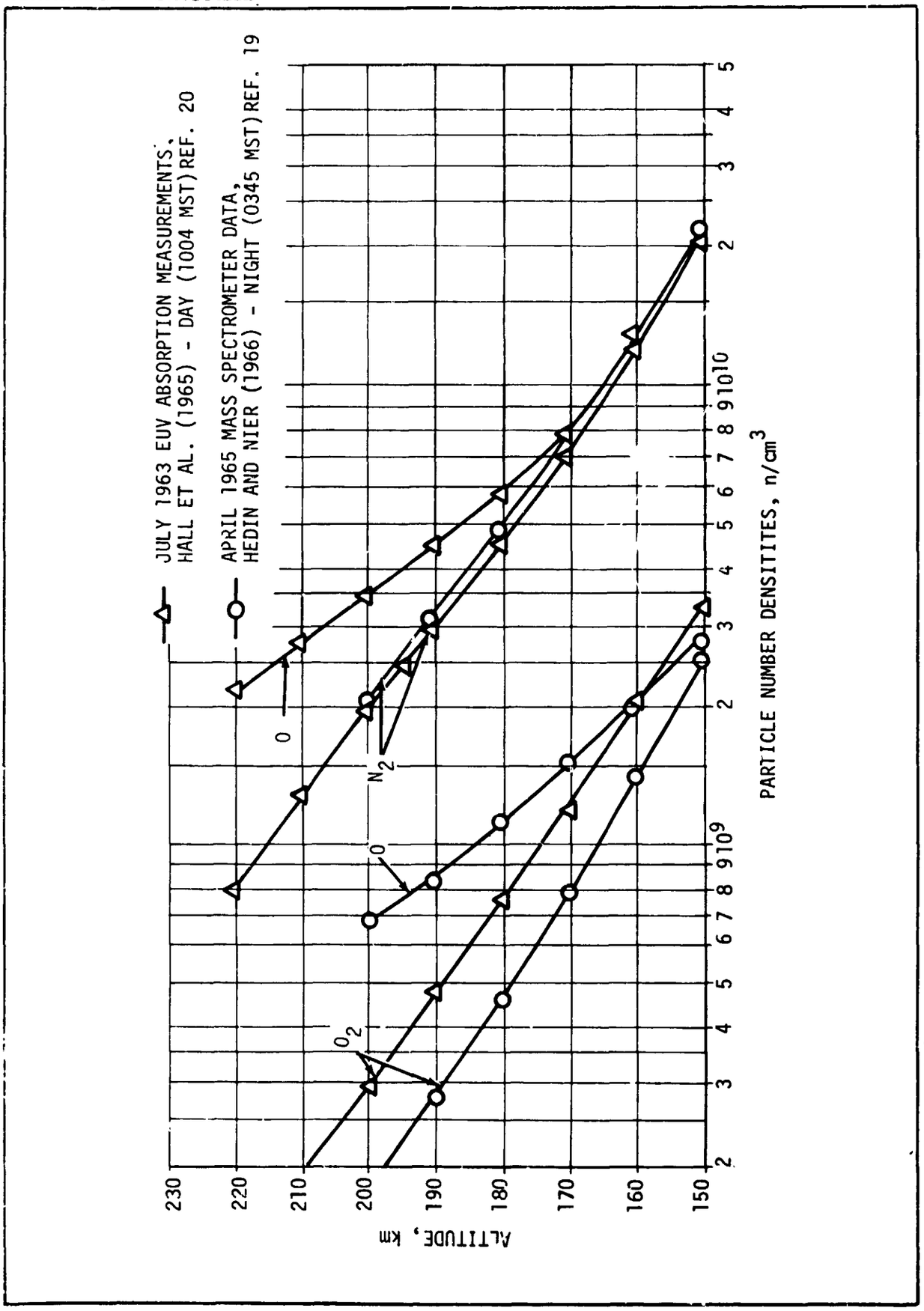

Figure 4-3. SELECTED PARTICLE NUMBER DENSITIES OF THE UPPER ATMOSPHERE FROM 150-220 KM

at 1004 hours MST. The greatest difficulty encountered with making adequate atmospheric composition measurements using the solar EUV absorption technique is due to the inadequate knowledge of the absorption cross sections. This is especially true for atomic oxygen measurements (ref. 30).

Figures 4-1, 4-2, and 4-3 also compare the EUV and mass spectrometer data. It is noted that the atomic oxygen number densities show the greatest disagreement among the data curves. Again the reader is referred to ref. 30 for a more detailed discussion.

4.1.2 Thermosphere Probes

The Thermosphere Probe series of mass spectrometer and Langmuir probe measurements was launched into the thermosphere over Wallops Island, Virginia during the 1962 to 1964 period (Spencer, et al., 1965, ref. 52 and Walters, et al., 1968, ref. 30). This series consisted of four flights of ejectable instruments designed to measure the concentration and temperature of N_2 and electrons under various conditions during a period approaching solar minimum. Figure 4-4 compares the N_2 particle number densities with mass spectrometer data and the CIRA 1965 model atmosphere. It is noted that the measured N_2 values are lower than the model atmosphere values by a factor of 2 (Figure 4-4). For reasons unknown at present, these results are typical because drag deduced densities are generally a factor of 2 higher than densities measured directly by in situ instruments.

4.1.3 The Explorer 17 Aeronomy-Aerodynamic Satellite

The aeronomy-aerodynamic satellite Explorer 17 (Spencer, ref. 53) was flown in the altitude range of 257 to 900 km and provided 50 hours of satellite operation over a period of 100 days. The satellite was launched on 3 April 1963 and provided data for various local times, altitudes, and geographic locations (between North and South latitudes of 58°). Although Explorer 17 operated at higher perigee altitudes than are proposed for the ODYSSEY I experiment, several of the observations derived from the Explorer 17 data are pertinent to a more complete understanding of the atmosphere in the 130 to 250 km altitude range. If the relative density measurements observed by Explorer 17 can be considered correct, the density showed a variation of a factor of 4 at 270 km and a factor

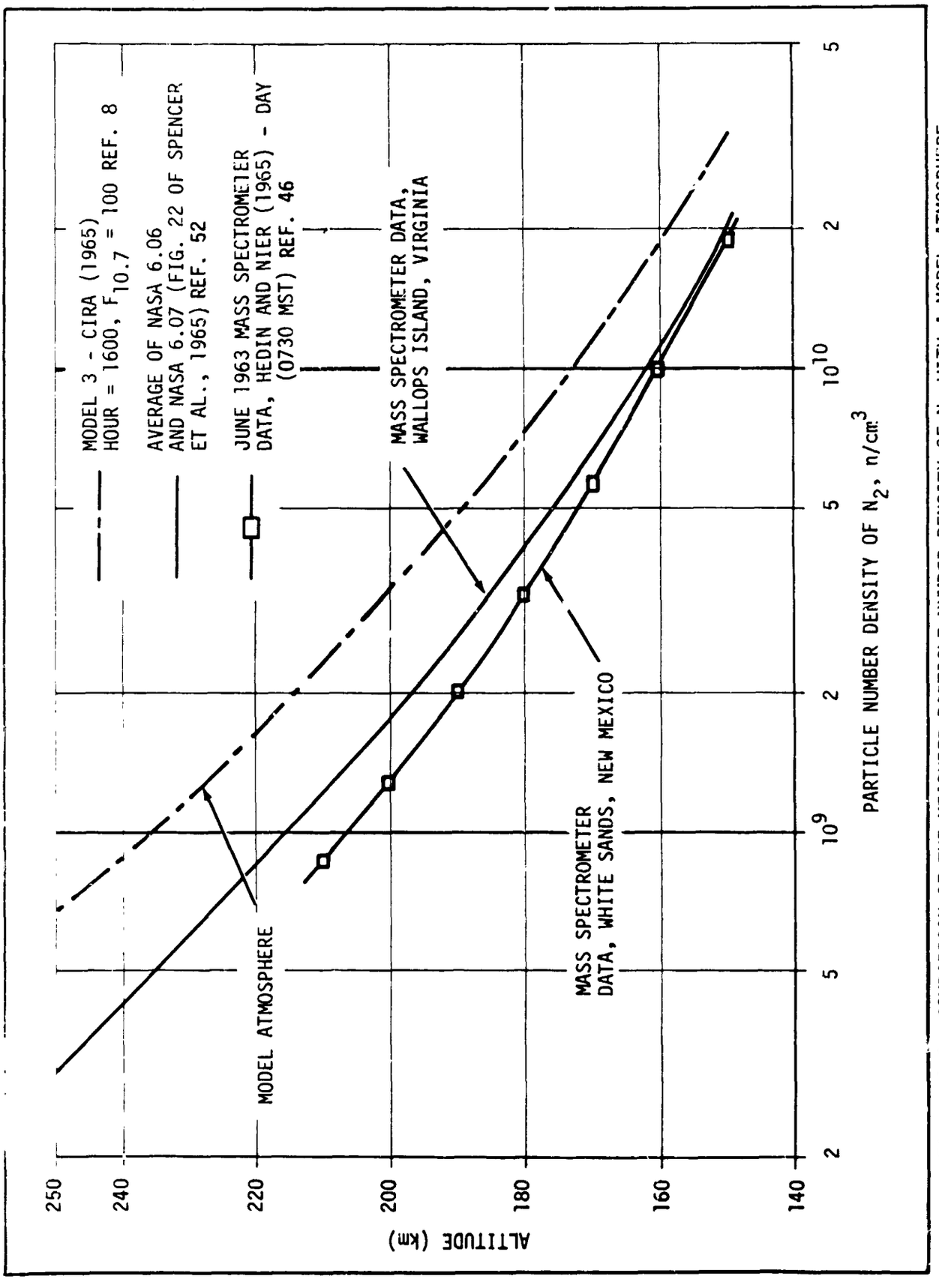

Figure 4-4. COMPARISON OF THE MEASURED PARTICLE NUMBER DENSITY OF N_2 WITH A MODEL ATMOSPHERE

of 10 at 450 km altitude. At 360 km altitude, the average density had a diurnal variation of a factor of 5 with a maximum value between 1200 and 1500 hours (Newton, et al., 1965, ref. 54). The present model atmospheres predict much smaller variations and, of course, no latitudinal variations at all. Drag deduced densities from spherical satellites or other pieces of orbital debris do not show these variations. Thus, it is possible and even probable that significantly larger variations than predicted by the model atmospheres extend all the way down through the operational altitude of the ODYSSEY I experiment. It is interesting to note that the drag determined densities for Explorer 17 satellite were found to be a factor of 2 greater than the averaged gauge densities (Bryant, 1964, ref. 55).

4.1.4 ATCOS-II Experiment

The ATCOS-II (Atmospheric Composition Satellite) was sponsored by the AFCRL and designated as OV3-6. It was launched 4 December 1967 into a circular polar orbit at an altitude of 435 km and a 90° inclination. The orbit was achieved by a Scout vehicle. The satellite had a 219 pound payload and a 256 day lifetime. Its instrumentation consisted of two mass spectrometers, three ion density probes, and an impedance probe. Particle number densities, total mass density, ion density, electron density, and temperature irregularities were measured.

4.1.5 Simultaneous Density Measuring Experiments

Pelz, et al., January, 1969 (ref. 56), compared neutral thermosphere density and temperature measurements from six nearly simultaneous experiments. Two Bayard-Alpert type ionization gauges were launched from Wallops Island, Va., 2 March 1966 at 1300 EST. These gauges determined the neutral density and temperature from 150-450 km altitude. The Bayard-Alpert gauges pumped all the O in this altitude range and read only the N_2, O_2 and He number density. These values agreed with neutral mass spectrometers and a solar EUV extinction experiment obtaining similar data over the altitude range. Also, previous N_2 measurements from thermosphere probes under the same solar and geomagnetic conditions agreed with the other experiments. Also, the distribution of the neutral and ion composition, the electron concentration, the electron density, as well as the neutral density and temperature were obtained. In general, all

the measurements were in good agreement with one exception. The pressure gauge total density values were lower than the mass spectrometer values due to the loss of 0 by the pressure gauges.

4.1.6 Other Composition Experiments

Other pertinent atmospheric composition experiments are discussed in the following sections. These other experiments are connected with EUV sensing techniques or drag force measurements as a means of obtaining atmospheric density.

4.2 IN SITU MEASUREMENTS OF AERODYNAMIC DRAG FORCE

4.2.1 Falling Spheres

Inflated spheres have been launched from sounding rockets to determine atmospheric density by measuring drag forces. The drag can be inferred from tracking data (Pearson, 1964, ref. 57; Peterson, et al., 1965, ref. 17) or it can be inferred from accelerometer measurements (Faucher, et al., 1962, ref. 16; Faire and Champion, 1965 and 1966 ref. 15 and ref. 58). Peterson has obtained drag data for altitudes up to 120 km from trajectory data. The accelerometer data have been used to calculate a density-versus-altitude profile to 130 km. The time-of-flight for falling spheres is typically less than 10 minutes. It should be noted that falling-sphere experiments are limited in that spatial and temporal density variations cannot be determined from only one flight. Also, most falling-sphere experiments cannot cover the critical altitude region above 120 km. However, the available falling-sphere data do tend to corroborate the assumed C_D values and match well with satellite data.

4.2.2 The Air Force Cambridge Research Laboratory Cannonball Satellite

The Cannonball experiment or OV1-16 (LOADS-Low Altitude Density Satellite) was proposed by the Air Force Cambridge Research Laboratory (Champion, 1966, ref. 59; Office of Aerospace Research, USAF, 1968, ref. 60). The Cannonball satellite was a low altitude, density measuring experiment launched 11 July 1968. It reentered on 19 August 1968 after obtaining over 200 data acquisitions or 10 hours of data. The Cannonball satellite was spherical, 23 inches in diameter, weighed 600 lbs, had a density of 162 lbs/ft^3, and covered an altitude range of

128 to 320 km. Its spin rate was 1 rpm and increased to 5 rpm before decay. Its instrumentation consisted of three orthogonal triaxial acceleration sensing systems, a tracking beacon, and an antenna. The acceleration measurements, plus the satellites area to mass ratio, velocity, and drag coefficient, provides a continuous measurement of atmospheric density. Pressure and temperature measurements could then be deduced from the density. Density was also deduced indirectly by observing the orbital period changes via tracking. The LOADS or Cannonball satellite flew with the SPADES experiment, which is discussed in a subsequent subsection.

4.2.3 The LOGACS Experiment

The LOGACS (Low Orbital Accelerometer Calibration Satellite) was developed by the Aerospace Corporation, El Segundo, California and AFCRL to measure the non-conservative forces acting on the satellite. Then, from this force measurement, obtained by miniature electrostatic accelerometer (MESA) measurements, the atmospheric density was calculated. The LOGACS experiment was placed into a polar orbit in May, 1967. It had a four day continuous lifetime and provided 100 hrs of accelerometer data. During its lifetime it monitored a geomagnetic storm. The orbit of the LOGACS experiment was 148 by 357 km. The drag coefficient for this satellite was assumed and the deduced density values are believed accurate to $\pm$ 10 percent.

4.2.4 Drag Free Satellites

The Stanford Drag Free Satellite (Lange, 1964, ref. 61; Cannon, et al., 1966, ref. 26) contains a small spherical ball or proof mass inside a completely enclosed cavity of a larger satellite. The external satellite is instrumented with jet-activated translational control mechanisms that cause the external shell to always pursue the proof mass in such a manner that they will never touch. Since the cavity is closed, the proof mass is shielded from solar radiation pressure and gas drag. Thus, once the other disturbing forces are proven negligible or compensated for, the orbital fluctuations of the proof mass will be due solely to gravitational forces. Reference 30 (Walters, et al., August, 1968) presents a more complete discussion of the Stanford Drag Free Satellite.

The basic satellite is spherical, 27.5 inches in diameter and weighs 300 pounds. The spherical symmetry allows the drag forces to be independent of vehicle attitude. Solar cells are used for power. The internal structure consists of three toroidal gas containers surrounding a central cylinder which contains the proof mass and its sensor, control electronics, battery and power control unit, telemetry and receiving equipment, tape recorder, orbital clock and programmer, and a simple wobble damper. Six thrusters are located symmetrically between the toroids, their nozzles being flush with the vehicle skin. Earth sensors and the Sun aspect sensor are also installed in the skin. The proof mass is a two-inch sphere, and the position sensors are capacitive pick-off plates connected in a capacitance bridge.

Two of these drag free satellites are to be placed in polar orbits with 130- and 140-km perigees and 470- and 1000-km apogees, respectively. Fuel would be available for a drag-free lifetime of about 10 days or 150 orbits. The first satellite will be in a polar orbit of 130 km perigee near the equator and an apogee of 470 km. A 40° band of latitude for approximately 100 passes, or about seven days, will be covered. The second satellite will have a polar orbit of 140-km perigee near the equator and a 1000-km apogee. A 27° band of latitude for 150 passes, or about 10 days, will be covered. During the drag-free lifetime, the translational control system would cause the satellite to undergo a purely gravitational orbit unaffected by drag or other forces. At the end of the drag-free life of one (or both) satellites, the proof mass would be caged electrostatically to act as an accelerometer, and the system would then gather additional air-drag data for the remaining 55 to 200 orbits of the satellite's lifetime.

The primary satellite measurement is aerodynamic drag. During the sustaining (drag-free) flight, the drag on the vehicle is measured in three ways: (1) by sensing the thrust directly (one percent accuracy), (2) by monitoring gas valve opening and inferring thrust (to about 15-percent accuracy), and (3) by computing vehicle absolute acceleration between gas-jet firings from the three-dimensional measurement of proof mass position relative to the satellite. During the secondary electrostatically caged mode the quantity

measured would be attitude, but only an approximate measurement (6^{o}) is required and attitude is not controlled.

These measured data, together with the tracking network and telemetric data-recovery services, will yield the drag vector as a function of satellite location and altitude. The drag data will be used to deduce aerodynamic density and to subsequently improve aeronomical models. The density data will be coupled with simultaneous sounding-rocket point measurements and solar observations to improve the Earth's atmospheric model in the presence of solar events.

Some requirements are placed on the vehicle design to allow drag data to be readily converted to density data. The satellite should be nearly spherical in shape to insure the least uncertainty in conversion from drag to density and should be spin stabilized with the preferred spin axis coinciding with the maximum moment of inertia axis. Spin stabilization will allow simplified attitude determination, eliminate rate gyros from the translation control system, improve vehicle thermal control, and reduce the gas consumption in the sustaining mode. The maximum spin rate will be 1 rps.

Again, additional information on the Stanford Drag Free Satellite can be found in reference 30 (Walters, et al., 1968). Also, the Italian San Marco I Satellite, designed to measure continuous drag force and deduce density over a 200 to 300 km altitude range, is discussed by Broglio, 1966 (ref. 62) and Walters, et al., 1968 (ref. 30).

4.3 ATMOSPHERIC DENSITY AND DRAG FORCES REDUCED FROM SATELLITES

Drag-force measurements as determined by falling spheres, San Marco, or drag-free satellites are converted to density measurements when C_D is accurately known. Drag-free satellite measurements are estimated to give C_D to a 5 percent accuracy with an averaging distance of 4 km at perigee, increasing with altitude.

The drag coefficient, C_D, will be known to a probable accuracy of about 15 percent with an extreme bound of 33 percent at altitudes in the vicinity

of 120 km to 470 km (Cannon, et al., 1966, ref. 26). This C_D error band is supported by data from Explorer VI, falling spheres, low density tunnels, the San Marco satellite, numerous satellite orbital tracking deductions, and all theoretical studies. Explorer XVII density measurements, advanced as an indication of uncertainty in C_D, contend that of the discrepancy of 100 percent between the drag and gauge inferences of density, at least 67 percent must be due to gauge interpretation (Cannon, et al., 1966, ref. 26). Hopefully, the proposed aerodynamic experiments will narrow the C_D and ρ uncertainty bands.

As discussed previously, the 100 to 200 km altitude range has been only sparsely explored. Rocket flights are of short duration and sample only a highly localized region. The difficulty with orbital-decay measurements of satellites below 200 km is that their lifetimes are short and tracking is difficult because of the limited visibility and the large fluctuating air drag. Also, orbital decay gives only a single, averaged density measurement near perigee.

Simultaneous rocket measurements of atmospheric composition to supplement the density measurements of the drag-free satellite can also be made. Rockets would be launched to determine density and composition from the absorption of solar X-ray ultraviolet radiation. The new X-ray cross sections of Henke, 1966, (ref. 63) would be used and are said to be accurate to 1 percent. Other types of density measurements such as glow clouds, pressure gauges, mass spectrometers, and falling spheres could be used simultaneously.

A nearly instantaneous measurement of drag is made on the drag-free satellite primarily from the measured thrust impulse and ball-position data. The drag vector orientation may be determined to 5^o although only the magnitude of the drag is really necessary. To determine ρ a simple rapidly converging iterative technique is used. First, an initial value of ρ_1 is assumed for density and a corresponding C_{D_1} is chosen from Figure 2-9 which was discussed earlier. The measured ρC_D is divided by C_{D_1} to obtain ρ_2. Then C_D is corrected to C_{D_2}, and the process is repeated. The process converges rapidly because C_D is highly insensitive to ρ throughout the entire 120- to 470-km altitude range.

4.4 SOME RELEVANT EUV AND X-RAY EXTINCTION EXPERIMENTS

The Aerospace Corporation of El Segundo, California has developed several aeronomy and aerodynamic experiments of interest to the ODYSSEY investigators. These Aerospace experiments were on the Air Force satellites 1966-70A and 1966-111B or the NASA satellite 1966-110A. The experiments concerned particle measurements and optical measurements.

One such experiment was designed to measure low-energy particle fluxes and was launched on OV1-15 (SPADES-Solar Perturbation of Atmospheric Density Experimental Satellite) into a polar orbit in June, 1968. It will study the heating of the upper atmosphere by low-energy charged particles. It will also study the fluctuations of the atmospheric density, composition, and temperature in the region from 150 to 500 km. The main objective of the measurements will be to identify the agencies causing these fluctuations. Correlations will be sought between observed density changes and various energy sources measured in situ, including solar X-rays and UV, ionosphere-neutral coupling, charged particle precipitation, and geomagnetic heating. Additional information, as well as a more complete discussion of the above information is available from R. A. Becker, 1967 (ref. 64).

Another Aerospace Corporation experiment is a Solar U.V. Monitor proposed by F. A. Morse and A. B. Prag (private communication, January 1968, ref. 65) and Becker (ref. 64). This experiment monitors the solar flux while monitoring density. Hopefully it can separate the changes in atmospheric density due to UV changes from those due to other changes in energy fluxes.

The experiment consists of seven photo-diodes with selected windows and ion chambers which permit the absolute intensity of the solar UV to be monitored. A spinning satellite without a solar pointer is suitable. It weighs 5.1 lbs, draws 31 ma at 28 volts. It was launched in June, 1968.

Drs. Morse and Prag are also responsible for an upper atmosphere O_2 and O_3 density profile experiment. This instrument is a crossed grating spectrometer with fixed grating and detector positions. It includes its own small but highly accurate solar pointer.

The O_2 and O_3 density profiles are obtained by an attenuation of the transmitted light as the satellite crosses the terminator (satellite sunset and sunrise) and as the satellite-sun line passes through the earth's atmosphere. Three wavelengths for O_2 absorption are monitored to provide redundancy and increase the instruments' sensitivity. As the satellite moves through its orbit, successive data points are associated with different portions of the atmosphere resulting in a determination of the vertical O_2 and O_3 density profiles.

The altitudes over which the instrument will sense O_2 are roughly 120 to 300 km and 40 to 100 km for O_3. Calculations based on model atmospheres show that 90 percent of the absorption occurs in about a 1000 km of path so that the densities derived are averages over less than 1/6 degree of great circle (or combined latitude and longitude, depending on the orbit). The altitude resolution obtained is about 3 km. The weight is 17 pounds, the power is 70 ma at 28 volts for the pointer and 80 ma at 28 volts for the experiment proper. Stabilization is useful since the pointer must be able to find the sun and not be occulted by the satellite body. Spinning satellites are acceptable but power requirements of the pointer increase. This experiment was scheduled for launch in October, 1968.

The Aerospace Corporation Solar X-ray Bragg Spectrometer experiment was developed by Drs. Rugge and Walker. The objectives of this experiment are twofold. First, it will measure the shape and absolute flux in the solar spectrum from 1 to 25Å. Secondly, it will measure the density of the atmosphere between 125 km and 250 km by observing the extinction of selected X-ray emission lines by the earth's atmosphere. The Bragg spectrometer is quite complicated and requires a solar pointer, but it provides the only means of obtaining accurate intensity measurements of an emission line spectra. Three crystal filters are used to cover the necessary wavelength range.

The atmospheric extinction experiment is performed by four fixed crystal spectrometers which are set on strong emission lines. Careful selection of the emission lines will allow the extinction caused by oxygen and nitrogen to be computed separately. The extinction is related to a line integral through the atmosphere, the major contribution to this integral coming from the point in the path with minimum altitude.

The solar pointer required for this experiment weighs 25 pounds and draws 245 ma at 28 volts. The electronics package weighs 3 pounds and draws 35 ma at 28 volts (Becker, 1967, ref. 64 and Morse, et al., private communication, 1968, ref. 65).

4.5 OTHER METHODS OF ATMOSPHERIC DENSITY AND GAS-SURFACE INTERACTION STUDIES

4.5.1 The Coordinated Sciences Laboratory Spinning Satellite Experiment

An interesting satellite experiment has been proposed and studied by the Coordinated Science Laboratory (CSL) of the University of Illinois (Knoebel, 1966, ref. 66 and Karr, May, 1966, ref. 67) to provide data from which the absolute atmospheric density, aerodynamic drag coefficient, and the gas-surface interaction phenomena may be deduced.

Basically, a single passive spinning satellite is utilized and the atmospheric drag, spin slow down rate, and spin axis precession rate are measured. From these measurements, the following parameters may be deduced: the momentum accommodation coefficient of the satellite surface, the thermal accommodation coefficient of the satellite surface, and the absolute mass density. In addition, information regarding the desorption and degassing rate of the satellite surface, mass density at various altitudes, and the change in accommodation coefficients with roughening of the satellite's surface by meteorites may be obtained.

The CSL-GSI experiment involves measurement of the torque parallel to the spin axis of the spin stabilized satellite, the aerodynamic torque perpendicular to the spin axis, and the satellite drag. The parallel torque, T_{11}, causes a slow down of the spin rate and the perpendicular component of torque, $T_{\perp}$, causes a precession of the spin axis in inertial space. The data read out system, proposed by CSL for a passive gyro-satellite system, allows both the precession and spin rate of the satellite to be measured to the required accuracy by using sunlight reflected from mirrors on the satellite's surface. A cone-sphere combination was found to be suitable for this study. A characteristic length of about one meter, or less, is suitable.

Also, since the density ρ, the momentum accommodation coefficient α_D, and the thermal accommodation coefficient α_T all may vary with time, this change could also be measured. Thus, the change in these coefficients with time could be related to the outgassing and desorption rate of the satellite surface. Also, if the satellite lifetime and orbit were suitable, the effect of the roughening of the satellite surface by meteorites on α_D and α_T could be determined.

CSL has also studied the torque effects of meteorites, electric charge induced torque, solar pressure effects, and gravity gradient effects. These effects are either negligible or can be readily accounted for.

The satellite can be completely passive but must be initially spun-up and properly oriented. CSL has also considered the feasibility of using two satellites with different surface characteristics. The surface of one would be designed to assure a known momentum and/or thermal accommodation. Then measurements of the orbital decay and spin decay of both satellites would allow determination of the atmospheric density and both thermal and momentum accommodation coefficients of the test satellite surface. The gas-surface interaction model used in this study will be that postulated by Maxwell, 1890 (ref. 41) and extended by von Smoluchowski, 1898 (ref. 68), although other models are being considered.

An optical readout system is utilized to measure the spin axis precession of a completely passive gyro in orbit, to an accuracy of less than one second of arc per year. This optical system, employing sunlight reflected from mirrors on the satellite's surface, is used to measure the gyro spin axis orientation by ground stations. Cylindrical mirrors will be used on the satellite surface to provide continuous flashes of reflected light which can be photoelectrically counted and timed to measure the spin rate on each satellite pass. Also, the continuously reflected light would aid in the orbital tracking of the satellite, necessary for determination of the orbital parameters and orbital decay.

Currently, the CSL personnel are investigating the use of gas-surface interaction models other than that of Maxwell. Also, analytical studies are

underway to develop expressions for the drag, slow down rate, and precession of a single cone-sphere satellite. Other studies are concerned with the accuracy of drag measurements and satellite degassing and contamination effects. Knoebel, 1966 (ref. 66), Karr, 1966 (ref. 67), and Knoebel and Yen, 1967 (ref. 69), as well as CSL's progress reports from October, 1967 to date, provide further details of the CSL Spinning Satellite gas-surface interaction experiment.

4.5.2 A Gas-Surface Energy Transfer Experiment

An experiment designed to measure the kinetic energy flux of the upper atmosphere relative to a satellite, as well as the fraction of this energy transferred at normal incidence to certain target surfaces, has been proposed and developed by D. McKeown of the Faraday Laboratories, La Jolla, California (McKeown, et al., 1966, ref. 70 and McKeown and Dummer, 1968, ref. 71).

The measurements are made by four probes which can detect energy transfer between 10 $\mu W/cm^2$ and 0.1 $\mu W/cm^2$ by frequency change of temperature sensitive quartz crystals. The accuracy of the probe measurements (3 percent) and the precision of measurements (better than 1 percent) are maintained by periodic in flight calibration of the crystal sensors.

This experiment was launched in June, 1969 on the OGO-F satellite in the altitude range of 400 to 1100 km. The experimental data obtained will be used to determine the energy accommodation and drag coefficients of Al and Au in O and N_2, the main constituents of the upper atmosphere in this altitude range. The measured kinetic energy flux also allows determination of atmospheric density, its variation with time, and scale height by relating measurements of the energy flux to the satellite ephemeris.

For the measurement of the kinetic energy flux, a wedge shaped cavity is mounted on a quartz crystal and the incident beam gives up its energy by multiple collisions before escaping as a thermalized beam. Fundamental energy transfer measurements to Al (a low atomic weight metal) and Au (a high atomic weight metal) plated on the crystals are performed. The results of this experiment would provide information allowing more accurate predictions of density, satellite drag, and orbital decay.

In the analysis of this experiment a molecule impacting on a surface in a free-molecule flow at satellite velocities is considered. A fraction of its energy is transferred to the surface as heat and the molecule rebounds with a lower velocity. This amount of impact energy released as heat can be determined since the net energy transfer, in the form of heat, to the surface per unit area per second is

$$Q = NE_i \ (1 - E_r/E_i) \text{ in } W/cm^2 \ ,$$

where: N is the number of molecules striking the target per unit area per second; E_i is the incident molecular energy; E_r is the energy of the rebounding molecules; and $1-E_r/E_i$ is the energy accommodation coefficient, α, assuming that the incident molecular energy is much greater than the energy that a molecule would have if its temperature were completely accommodated to the target surface temperature. Detailed discussions of theoretical and experimental investigations of the energy accommodation coefficient at thermal energies may be found in Kaminsky, 1965 (ref. 72) and Dietz, 1965 (ref. 73).

Further analysis enables the rate of heat transfer per unit surface area for both N_2 and 0 to be calculated. Also the energy transfer probes will measure the impact energy of the incident molecules by monitoring the frequency change of a temperature sensitive quartz crystal. The test surface to be used in measurement is plated on the face of the crystal sensor.

The increase in the output frequency during bombardment is proportional to the transfer of energy by the incident molecular beam to the crystal sensor. A shutter is opened for about 100 seconds, allowing the incident beam to bombard the crystal. Since 100 seconds is sufficient time for an accurate measurement, the shutter is then closed so that the sensor can return to its ambient temperature and be ready for a new measurement. The shutter is made of a barium fluoride blank that has a wide IR window to minimize temperature changes of the crystal caused by differences in thermal radiation into space when the shutter steps from a closed to an open position. Also other precautions were taken to minimize heat loss by radiation from the crystal.

Basically, two types of sensors are used in the probes. One is an optically polished quartz crystal and is plated with either Al or Au for accommodation measurements. The other type of crystal sensor is fitted with a cavity for measuring the kinetic energy flux of 10 eV beams. The incident beam loses its energy by multiple collisions with the walls of the cavity before escaping as a thermalized beam.

The proper length of the probes was determined to minimize the view the sensor has of the free stream for good temperature stability but not affect the free-molecular-flow conditions inside the probe. The four probes with supporting electronics are housed in a single instrument package 4.5 x 7 x 7.5 inches, weighing 4.8 lbs, and operating at 28 Vdc at 3.5W. Probe (1) will measure energy transfer to an Al surface; Probe (2) is a control offset 13° from the velocity vector to determine its signal to noise ratio; Probe (3) will measure energy transfer to an Au surface; and Probe (4) will measure the kinetic energy flux of the upper atmosphere.

A laboratory calibration has been performed and the calibration constants should not change significantly because of the high stability of quartz crystals. However, the probes will be checked in orbit periodically. The operating temperature of the probes will be monitored in flight to maintain accuracy. From the measured values, the mean molecular weight of the upper atmosphere and the accommodation coefficients of Al and Au will be determined to accuracies of 3 percent.

This experiment will also allow the determination of the number density of O and its energy accommodation coefficient with the test surfaces at higher altitudes. These number densities will be found by the total kinetic energy probe with the help of the equation,

$$\bar{E} = (AV^3/2)\ (n_O\, m_O + n_{N_2} m_{N_2}) = (W_4\, C_p/\bar{k})\ \frac{dF_4}{dt},$$

where,

$\overline{E}$ = total kinetic flux of the upper atmosphere

$W_4 C_p$ = heat capacity of the sensor (Probe 4)

$\frac{dF_4}{dt}$ = change in output frequency with time for Probe (4).

m = mass of gas component

n = number density of gas component

O = atomic oxygen

N_2 = nitrogen

A = surface area

V = satellite velocity

$\overline{k}$ = frequency-temperature dependence $\frac{dF}{dT} \approx 1500 \frac{Hz}{^oC}$.

Also, the density, pressure scale height , temperature, and the drag coefficient for Al and Au will be deduced.

Again, additional details are available from McKeown, et al., 1966 (ref. 70) and McKeown and Dummer, 1968 (ref. 71).

Section V

CONCLUSIONS AND RECOMMENDATIONS

5.1 CONCLUSIONS

From the preceding study of the ODYSSEY I experiment package and a comparison with other aerodynamic and aeronomy experiments, the following conclusions may be made:

- Uncertainties remain in the values of the free-molecular-flow drag coefficient and the near-free-molecular-flow drag coefficient, with an uncertainty band of $\pm$ 30 percent for the free-molecular-flow case.
- Understanding of the gas-surface interaction phenomena is not yet complete, especially under the conditions of satellite energies and surface contamination conditions.
- The Coordinating Science Laboratories satellite, the Faraday Laboratories GSI experiment, and the University of Michigan GSI experiment all appear to be promising methods of determining energy accommodation in situ.
- Knowledge of the upper atmosphere between 120 km and 240 km is indeed very poor, especially regarding spatial and temporal density variations.
- A factor of 1.5 to 2 persists between drag-deduced densities and densities obtained by in situ instrumentation.
- Past aeronomy or aerodynamic experiments have not been able to provide a complete and systematic coverage of any portion of the upper atmosphere for different conditions of solar activity, geomagnetic storms, and other short-term or long-term variations.
- The proposed ODYSSEY I experiment package would provide a systematic investigation of the upper atmosphere between 140 and 240 km during the forthcoming period of high solar activity.

5.2 RECOMMENDATIONS

The following recommendations are made in an effort to provide a more systematic evaluation of satellite interactions with the earth's upper atmosphere:

- Concentration measurements of O, O_2, and N_2 should be made by as many density determining techniques as possible at the same time and place in orbit. In other words, EUV extinction measurements, mass spectrometer measurements, gauge measurements, and density measurements deduced by tracking should all be performed simultaneously, if and

whenever possible. This recommendation is made in view of "the atomic oxygen problem" and since cross calibration between any two of the density determining techniques given above is needed.

- It is strongly recommended that additional laboratory programs be instituted to investigate the production, calibration, and isolation of atomic oxygen.
- A more systematic coverage of the aerodynamic and aeronomical parameters of upper atmospheric flight could be accomplished by closer cooperation between the many experimenters in this field. It is recommended that an ambitious program such as the ODYSSEY I experiment take advantage of any other experiments or concepts that will enhance its ability to provide useful, accurate, and complete data.

Section VI

REFERENCES AND BIBLIOGRAPHY

1. Von Zahn, U., "Mass Spectrometric Measurements of Atomic Oxygen in the Upper Atmosphere: A Critical Review," J. Geophys. Res., Vol. 72, No. 23, December 1, 1967.
2. Kasprzak, W. T., et al., "A Study of Day-Night Variations in the Neutral Composition of the Lower Thermosphere," J. Geophys. Res., Vol. 73, No. 21, Nov. 1, 1968.
3. Krankowsky, D., et al., "Mass Spectrometric Studies of the Composition of the Lower Thermosphere During Summer 1967," J. Geophys. Res., Vol. 73, No. 23, Dec. 1, 1968.
4. Ariel II, "Ariel II Engineering Data Analysis," Phase III Final Report, Westinghouse Electric Corp, Baltimore, Md., 1965.
5. Stewart, K. H. ard Miller, D. E., "Preliminary Results from Ozone Experiments in the Ariel II Satellite," (unpublished).
6. Reiter, G. S., "Free-Molecule-Flow and Particle-Surface Interactions," (unpublished).
7. Vigneron, F. R. and Garrett, T. W., "Solar Induced Distortion Atmospheric Drag Coupling in Alouette Satellites," Defense Research Telecommunications Establishment DRTE 1171, February 1967.
8. Cospar International Reference Atmosphere (CIRA) 1965, North-Holland Publishing Company, Amsterdam, 1965.
9. United States Standard Atmosphere Supplement 1966 (USSAS), COESA, Government Printer, Washington, D.C., 1966.
10. King-Hele, D. G. and Quinn, E., "Upper-Atmosphere Density, Determined from the Orbits of COSMOS ROCKETS," Planetary and Space Science, Vol. 14, 1966, pp. 1023-1033.
11. Priester, W., "On the Variations of the Thermospheric Structure," Proc. Royal Soc. London, A, Vol. 288, 1965, pp. 493-509.
12. Cook, G. E., "On the Accuracy of Measured Values of Upper-Atmosphere Density," J. Geophys. Res., Vol. 70, No. 13, 1965, p. 3242.
13. Moe, O. K., Institute of Geophysics and Planetary Physics, UCLA, L. A., California, private communication, 12 August 1967.
14. Bartman, F. L., Chaney, L. W., Jones, L. M., and Lin, V. C., "Upper-Air Density and Temperature by the Falling-Sphere Method," J. Appl. Phys., Vol. 27, No. 7, 1956.
15. Faire, A. C. and Champion, K. S. W., "Falling-Sphere Measurements of Atmospheric Density, Temperature, and Pressure up to 115 km," Space Research V, 1965, p. 1039.
16. Faucher, G. I., Procunier, R. F., and Sherman, F. S., "Upper Atmospheric Density Obtained from Measurements of Drag on a Falling Sphere," AFCRL-62-1136, J. Geophys. Res., Vol. 68, No. 11, June 1963, pp. 3437-3750.

17. Peterson, J. W., Hansen, W. H., McWatters, K. D., and Bonfanti, G., "Falling Sphere Measurements over Kwajalein," J. Geophys. Res., Vol. 70, No. 18, 1965, pp. 4477-4489.

18. NASA, U. S. Standard Atmosphere, Washington, D.C., 1962.

19. Hedin, A. E. and Nier, A. O., "A Determination of the Neutral Composition, Number Density, and Temperature of the Upper Atmosphere from 120 to 200 Kilometers with Rocket-Borne Mass Spectrometer," J. Geophys. Res., Vol. 71, No. 17, 1 September 1966, pp. 4121-4131.

20. Hall, L. A., Schweizer, W., and Hinteregger, H. E., "Improved Ultraviolet Absorption Measurements in the Upper Atmosphere," J. Geophys. Res., Vol. 70, No. 1, 1 January 1965, pp. 105-111.

21. Horowitz, R., "Direct Measurements of Density in the Thermosphere," Ann. Geophys., Vol. 22, 1966, pp. 31-39.

22. Taeusch, D. R., et al., "Diurnal Survey of the Thermosphere," Univ. of Mich., College of Engineering, Final Report, ORA Project 07446, October, 1967.

23. Taeusch, D. R., et al., "Diurnal Survey of the Thermosphere," NASA CR-61481, November, 1968.

24. Hung, F. T. and Lou, G. S., "Thermospheric Temperature Model Deduced From Mass Spectrometric Measurements," Presented at AGU 50th Annual Meeting, April 21-25, 1969, Washington, D.C., Paper No. STA-55.

25. Weidner, D. K. and Swenson, G. R., "Diurnal Variations in the Thermosphere From a Series of Marshall-University of Michigan Probes," to be published, JGR, August, 1968.

26. Cannon, R. H., et al., "Proposal to Develop and Operate a Sustaining Earth Satellite in Two Orbital Flights," Dept. of Aeronautics and Astronautics, Stanford University, February 1966 (with Addendum, September 1966).

27. Nocilla, S., "On the Interaction between Stream and Body in Free-Molecule-Flow," Rarefied Gas Dynamics, Second Symposium, Academic Press, New York, 1961.

28. Nocilla, S., "The Surface Re-Emission Law in Free-Molecule-Flow," Rarefied Gas Dynamics, Third Symposium, Academic Press, New York, 1963.

29. Schamberg, R., "Analytic Representation of Surface Interaction for Free Molecule Flow with Application to Drag of Various Bodies," Project Rand Aerodynamics of Upper Atmosphere, R-399, 1959.

30. Walters, W. P., et al., "Evaluation of ODYSSEY I and Related Aerodynamical and Aeronomical Experiments," Nortronics-Huntsville Technical Report No. 391, TR-792-8-386, August, 1968.

31. Moe, O. K., "Atmospheric Densities Determined From the Spin Decay of Explorer VI," Ph.D. Dissertation, Department of Planetary and Space Physics, UCLA, L. A., California, 1966.

32. Lundquist, C. A., Lam, L. S., and Mendes, G. M., "Design of a Satellite Experiment for Atmospheric Density and Near-Free-Molecular-Flow Aerodynamics," Draft of a Report Prepared under NsG87-60 for the National Aeronautics and Space Administration, 1967.

33. Maslach, G. J., Willis, D. R., Tang, S., and Ko, D., "Recent Experimental and Theoretical Extensions of Nearly Free Molecule Flow," Rarefied Gas Dynamics, Fourth Symposium, Academic Press, New York, 1964.

34. Cook, G. E., Annales de Geophysique, Vol. 22, 1966, p. 53.

35. Sterne, T. E., "An Atmospheric Model, and Some Remarks on the Inference of Density from the Orbit of a Close-Earth Satellite," Astronaut. J., Vol. 63, No. 3, March 1958.

36. Jacchia, L. G. and Slowey, J., "Formulae and Tables for the Computation of Lifetimes of Artificial Satellites," SAO Special Report No. 135, 1963.

37. Moe, O. K., "Accommodation and Drag Coefficients Derived from the Spin and Orbital Decays of Paddlewheel Satellites," Institution of Geophysics and Planetary Physics, UCLA, L. A., California, 1966.

38. Moe, O. K., "Absolute Atmospheric Densities Determined from the Spin and Orbital Decays of Explorer VI" COSPAR, International Space Science Symposium, 7th, Vienna, Austria, 1966.

39. King-Hele, D. G., Theory of Satellite Orbits in an Atmosphere, Butterworths, London, 1964.

40. Alcalay, J. A. and Knuth, E. L., to be published in Rarefied Gas Dynamics, Fifth Symposium, Academic Press, New York, 1966.

41. Maxwell, J. C., The Scientific Papers of James Clerk Maxwell, Vol. 2, Cambridge University Press, 1890.

42. Zorn, J. C., et al., "A Feasible Satellite Experiment For Gas Molecule-Solid Surface Interaction Studies," Univ. of Mich., College of Engineering, Final Report, ORA Project 08700, October 1967.

43. Leite, R. J., "Environmental Composition," Proposal for an Apollo Earth Orbital Scientific Experiment, High Altitude Engineering Laboratory, University of Michigan, (undated).

44. SDS Aerospace Systems, "Introduction to Mass Spectrometry," Pomona, California, 1966.

45. Nier, A. O., Hoffman, J. H., Johnson, C. Y., and Holmes, J. C., "Neutral Composition of the Atmosphere in the 100- to 200-Kilometer Range," J. Geophys. Res., Vol. 69, 1964, pp. 979-989.

46. Hedin, A. E. and Nier, A., "Diffusive Separation in the Upper Atmosphere," J. Geophys. Res., Vol. 70, No. 5, 1965, pp. 1273-1274.

47. Hedin, A. E., Avery, C. P., and Tschetter, C. D., "An Analysis of Spin Modulation Effects of Data Obtained with a Rocket-Borne Mass Spectrometer," J. Geophys. Res., Vol. 69, 1964, pp. 4637-4648.

48. Hinteregger, H. E., "Telemetering Monochromatic Measurements of Extreme Ultraviolet Radiation," Space Astrophysics, edited by W. Liller, McGraw-Hill Book Company, New York, 1961, pp. 34-95.

49. Hinteregger, H. E., "Preliminary Data on Solar Extreme Ultraviolet Radiation in the Upper Atmosphere," J. Geophys. Res., Vol. 66, 1961, pp. 2367-2380.

50. Hall, L. A., Damon, K. R., and Hinteregger, H. E., "Solar Extreme Ultraviolet Photon Flux Measurements in the Upper Atmosphere of August 1961," Space Research III, North-Holland Publishing Company, Amsterdam, 1963, pp. 745-759.

51. Nier, A. O., "The Neutral Composition of the Thermosphere," Ann. Geophys., Vol. 22, 1966, pp. 102-109.

52. Spencer, N. W., Brace, L. H., Carignan, G. R., Taeusch, D. R., and Niemann, H., "Electron and Molecular Nitrogen Temperature and Density in the Thermosphere," J. Geophys. Res., Vol. 70, No. 11, 1965, pp. 2665-2698.

53. Spencer, N. W., "The Explorer XVII Satellite," Planetary and Space Science, Vol. 13, 1965, pp. 593-598.

54. Newton, G. P., Horowitz, R., and Priester, W., "Atmospheric Density and Temperature Variations from the Explorer XVII Satellite and Further Comparison with Satellite Drag," Planetary and Space Science, Vol. 13, 1965, pp. 599-616.

55. Bryant, R., "Densities Obtained From Drag on the Explorer XVII Satellite," J. Geophys. Res., Vol. 69, No. 7, 1964, pp. 1423-1425.

56. Pelz, D. T., et al., "Midlatitude Neutral Thermosphere Density and Temperature Measurements," J. Geophys. Res., Vol. 74, No. 1, January 1969.

57. Pearson, P. H. O., "Basic Atmospheric Parameters as Measured by Four Falling Sphere Experiments at Woomera December 1964-March 1965," Technical Note Pad No. 109, NASA Accession No. N66-21743, 1964.

58. Faire, A. C. and Champion, K. S. W., "High Altitude Rocket Density Measurements at Eglin, Florida," Space Research VI, 1966.

59. Champion, K. S. W., "Satellite to Measure Air Density Planned," Aviation Week and Space Technology, 7 November 1966, p. 89.

60. Office of Aerospace Research, USAF, VII, No. 8, August 1968.

61. Lange, B. O., "The Drag-Free Satellite," AIAA J., Vol. 2, No. 9, September 1964.

62. Broglio, L., "Air Density Between 200 and 300 km Obtained by San Marco I Satellite," Space Research VII, North-Holland Publishing Company, Amsterdam, 1966, pp. 1135-1147.

63. Henke, B., "Cross Sections of Atmospheric Gases in the Soft X-Ray Region," (to be published), 1966.

64. Becker, R. A., "Space Physics Laboratories Summary of Space Research," submitted to COSPAR CY 1967, Aerospace Corp., L. A., Calif., June 1968.

65. Private Communication, Drs. F. A. Morse, A. B. C. Walker, H. R. Rugge, and A. B. Prag, Aerospace Corporation, L. A., Calif., Jan. 15, 1968.

66. Knoebel, H. W., "Proposal for Feasibility Study for an Orbital Density, Drag Coefficient, Gas-Molecule Surface Interaction Experiment," Coordinated Science Laboratory, University of Illinois, Urbana, Illinois, 14 October 1966.

67. Karr, G. R., "Aerodynamic Torque on a Spinning Spherical Satellite with Application to Measurement of Accommodation Coefficients," Coordinated Science Laboratory Report R-295, University of Illinois, Urbana, Illinois, May 1966.

68. von Smoluchowski, Weid Arn., Vol. 64, 1898, p. 101.

69. Knoebel, H. W. and Yen, S., "Study of an Orbital Gyroscopic Experiment to Measure Gas Density and Gas Molecular Surface Interaction Parameters," A Proposal from the Coordinated Science Laboratories, University of Illinois, Urbana, Illinois, November 1967.

70. McKeown, D., Carlston, C. E., Poppa, H. R., and Fox, M. G., "Gas-Surface Interactions," Annual Report of the Space Science Laboratory GDC-DBE-66-016, General Dynamics Convair, San Diego, California, October 1966.

71. McKeown, D. and Dummer, R. S., "Gas-Surface Energy Transfer Experiment For OGO-F," to be published, IEEE Geoscience Electronics, 1969.

72. Kaminsky, M., Atomic and Ionic Impact Phenomena on Metal Surfaces, Academic Press, New York, 1965.

73. Dietz, V. R., Ind. Eng. Chem. (USA), Vol. 57, 1965, p. 49.

74. Schaaf, S. A. and Chambre, P. L., "Flow of Rarefied Gases," High Speed Aerodynamics and Jet Propulsion, Vol. 4, Part G, Princeton University Press, Princeton, N. J., 1958.

75. Lundquist, C. A., et al., "Design of a Satellite Experiment for Atmospheric Density and Near-Free-Molecular-Flow Aerodynamics," SAO Special Report No. 241, June 5, 1967.

76. Kinslow, M. and Potter, J. L., "Drag of Spheres in Rarefied Hypervelocity Flow," AIAA J., Vol. 1, No. 11, 1963, pp. 2467-2473.

77. Escobal, P. R., Methods of Orbit Determination, John Wiley & Sons, N.Y., 1965.

78. Leite, R. J., Mason, C. J., and Kistler, R. D., "Instrument Report, Neutral and Ion Mass Spectrometer," High Altitude Engineering Laboratory, University of Michigan, Report No. 05465-1-T, 1964.

79. Nier, A. O., "Mass Spectrometry of the Neutral Constituents of the Upper Atmosphere," Mass Spectroscopy, (Society of Mass Spectroscopy of Japan), Vol. 15, No. 2, 1967.

80. Kallmann-Bijl, H. K. and Sibley, W. L., "Diurnal Variation of Temperature and Particle Density Between ≈100 km and ≈500 km," Space Research IV, North-Holland Publishing Company, Amsterdam, 1964, pp. 279-301.

81. Bungiorno, C. and Trella, M., "Considerations of the Drag Coefficient for the San Marco Satellite," Atti del Centro Ricerche Aerospaziali, 1964.

82. Champion, K. S. W., "Variation with Season and Latitude of Density, Temperature and Composition in the Lower Thermosphere," Presented at the COSPAR 7th International Space Science Symposium, Vienna, May, 1966.

83. Knudsen, M., Ann. Physik. 34, 1911, p. 593.

Appendix A

NEAR-FREE-MOLECULAR-FLOW DRAG COEFFICIENTS

The form of most theoretical expressions for near-free-molecular-flow drag coefficients for spheres is (Maslach, et al., 1964, ref. 33)

$$C_D = C_{D_{fm}} - \frac{1}{Kn} F\,(S_b, S_\infty) \qquad \text{(A-1)}$$

where $C_{D_{fm}}$ is the value of the drag coefficient for free molecular flow, Kn is the free-stream Knudsen number (free-stream mean free path/sphere diameter), S_b is the molecular speed ratio of the gas diffusely emitted from the surface, and S_∞ is the molecular speed ratio for the free stream.

The value of the function $F(S_b, S_\infty)$ has taken various forms, although Maslach, et al. (ref. 33) have concluded that the following expressions give the best agreement with laboratory data:

$$F = (0.165\, S_b + 1.44 - 1.13/S_b)/S_\infty \quad \text{(Willis, see ref. 33)} \qquad \text{(A-2)}$$

$$F = (0.33\, S_b - 0.12)S_\infty \quad \text{(Rose, see ref. 33)} \qquad \text{(A-3)}$$

The aerodynamic drag per unit mass (D/m) of the satellite may be written as

$$\frac{D}{m} = \frac{1}{2} C_D \frac{A}{m} V^2 \rho = \frac{1}{2} \left[C_{D_{fm}} - B\, F(S_b, S_\infty)\, d\, \rho \right] \frac{A}{m} \rho V^2 \qquad \text{(A-4)}$$

where $B = \sqrt{2}\ \pi \sigma_c^2 N_o / W$, σ_c is the effective collision diameter of a molecule of air, N_o is Avogadro's number ($N_o = 6.02 \times 10^{23}$ molecules/g mole), W is the mean molecular weight of the air molecules, and m is the mass of the sphere.

Most of the quantities in equation (A-4) can be considered known or easily measured from the tracking data. The exceptions are the coefficient of drag for the free-molecular regime, $C_{D_{fm}}$, the atmospheric density, ρ, and the values of $F(S_b, S_\infty)$. If the value for $C_{D_{fm}}$ can be taken from the relation

$$C_{D_{fm}} = 2 + 1.18/S_b \qquad \text{(A-5)}$$

then, only the atmospheric density, ρ, and the values of $F(S_b, S_\infty)$ remain to be determined from appropriate analysis of tracking data. Equation (A-5) is taken for diffuse reflection from Schaaf and Chambre, 1958, (ref. 74) as suggested by Lundquist, et al., 1967 (ref. 75).

All theories agree that the first small departure of C_D from the free-molecular-flow value is proportional to the ambient molecular number density, the inter-molecular collision cross section, the sphere diameter, and to a representative ratio of the density of scattered molecules to the ambient density. When a consistent convention relating this density ratio to the wall temperature and flight velocity of the sphere is applied to all theories, the differences between them appear as contradictory predictions regarding the proportionality factor and secondary effects of the sphere temperature. It is not yet possible to justify any given theory, but at 120 km the range of theoretical C_D values is 1.45 to 2.35 (Cannon, et al., 1966, ref. 26).

Kinslow and Potter, 1963 (ref. 76) obtained some near-free-molecular-flow data on spheres and determined $C_{D_{fm}} - C_D$ as a function of the Reynolds number and n_r/n_∞. In this case n_r and n_∞ are the number densities of the reemitted and incident molecules, respectively. Only rough estimates of the effects of different reemission models on $C_{D_{fm}} - C_D$ can be determined by looking at their effects on n_r/n_∞. The use of Nocilla's model (Nocilla, 1961 and 1963, ref. 27 and ref. 28) shows n_r/n_∞ to be sensitively dependent on both the thermal accommodation coefficient and the tendency toward specular reflection. In particular, n_r/n_∞ decreases very rapidly in response to small deviations from the normally assumed case of completely diffuse reemission and complete energy accommodation.

Similar techniques exist for predicting the aerodynamic drag coefficient of other common shapes (e.g., cylinder, two-dimensional flat strip, etc., Maslach, et al., 1964, ref. 33).

Appendix B

DERIVATION OF THE EQUATION FOR THE RATE OF CHANGE OF ORBITAL PERIOD WITH RESPECT TO TIME

The rate of change of the orbital parameters with respect to eccentric anomaly may be written as (Escobal, 1965, ref. 7):

$$\left(\frac{da}{dE}\right)_D = -2b\rho\, a^2 \frac{(1 + e\cos E)^{3/2}}{(1 - e\cos E)^{1/2}} \left[1 - d' \frac{(1 - e\cos E)}{(1 + e\cos E)}\right]^2 \qquad \text{(B-1)}$$

$$\left(\frac{de}{dE}\right)_D = -2b\rho\, a(1-e^2) \left[\frac{1 + e\cos E}{1 - e\cos E}\right]^{1/2} \left[1 - d' \frac{(1 - e\cos E)}{(1 + e\cos E)}\right]$$

$$\left\{\cos E - \frac{d'}{2}(1-e^2)^{-1} (1-e\cos E)(2\cos E - e - e\cos^2 E)\right\} \qquad \text{(B-2)}$$

$$\left(\frac{di}{dE}\right)_D = -\frac{1}{2} b\,\rho a\,\omega_s \frac{\sin i}{\hat{n}} (1-e^2)^{-1/2} (1 - \cos 2u)$$

$$(1 - e\cos E)^{5/2} \left\{ (1 + e\cos E)^{1/2} \left[1 - d' \frac{(1 - e\cos E)}{(1 + e\cos E)}\right]\right\} \qquad \text{(B-3)}$$

where

$$b = \frac{C_D A}{2m}$$

and

$$d' = \frac{\omega_s}{n} (1-e^2)^{1/2} \cos i.$$

The orbital period P_o, is given as,

$$P_o = \frac{2\pi}{k\mu^{1/2} a^{-3/2}}$$

The pertinent symbols used in the above equations are given below:

A = satellite effective drag area

a = semimajor axis

C_D = drag coefficient

E = perturbed eccentric anomaly

e = eccentricity

$\imath$ = inclination

k = gravitational constant

$M = E - e \sin E$ = mean anomaly

m = satellite mass

$\hat{n}$ = anomalistic mean motion

P_o = orbital period

μ = sum of earth and satellite masses

ρ = atmospheric density

ρ_p = atmospheric density at perigee

ω_s = planetary rotation rate.

The eccentric anomaly values used include secular variations due to gravitational anomalies. The subscript D indicates secular rates of change due to drag.

The rate of change of the semimajor axis with the perturbed eccentric anomaly, $\frac{da}{dE}$, is directly related to the rate of change of orbital period with respect to time. Then, using equations (B-1) and (B-4) and assuming

$$\left(\frac{\omega_s}{\hat{n}} (1-e^2)^{1/2} \cos i \frac{(1 - e \cos E)}{(1 + e \cos E)}\right) << 1,$$

the rate of change of the orbital period with time of any of the passive spheres may be written as,

$$\frac{dP}{dt} = - \frac{3}{2} \frac{A}{m} \rho_p a \int_o^{2\pi} C_D \frac{\rho}{\rho_p} \frac{(1 + e \cos E)^{3/2}}{(1 - e \cos E)^{1/2}} dE.$$

which is equation (2) in subsection 3.1.2. Note that the near-free-molecular-flow drag coefficient, C_D, was removed from the integral sign in subsection 3.1.2. Thus C_D is assumed to be independent of E, the perturbed eccentric anomaly. The density at perigee ρ_p, was also assumed to independent of E.

Appendix C

SCHAMBERG'S ACCOMMODATION MODEL

In Schamberg's drag and accommodation coefficient model (Schamberg, 1959, ref. 29) the following assumptions are employed when applied to paddlewheel satellites:

- Free molecular flow exists.
- The angle between the satellite velocity vector and spin vector is less than 33 degrees.
- No air molecules strike the satellite more than once.
- The only important torques are caused by air molecules striking the paddles.
- Air molecules have no random thermal motion due to the high satellite velocity.

Schamberg relates the angle of incidence, θ_i, to the angle of reflection, θ_r, by the equation

$$\cos\theta_r = (\cos\theta_i)^{\nu}, \quad \nu \geq 1 \tag{C-1}$$

$\nu = 1$, specular reflection

$\nu = \infty$, diffuse reemission.

Schamberg also determines the speed of reemission, V_r, as related to the incident speed, V_i, as

$$\frac{V_r}{V_i} = \sqrt{\frac{T_r}{T_i}} = \sqrt{1 + \alpha\left(\frac{T_w}{T_i} - 1\right)} \tag{C-2}$$

By adding incident and reemitted momentum fluxes and dividing by half the incident flux, obtain

$$C_D = 2 \left[1 + \phi(\phi_o) \frac{V_r}{V_i} f(\nu, \text{shape})\right] \tag{C-3}$$

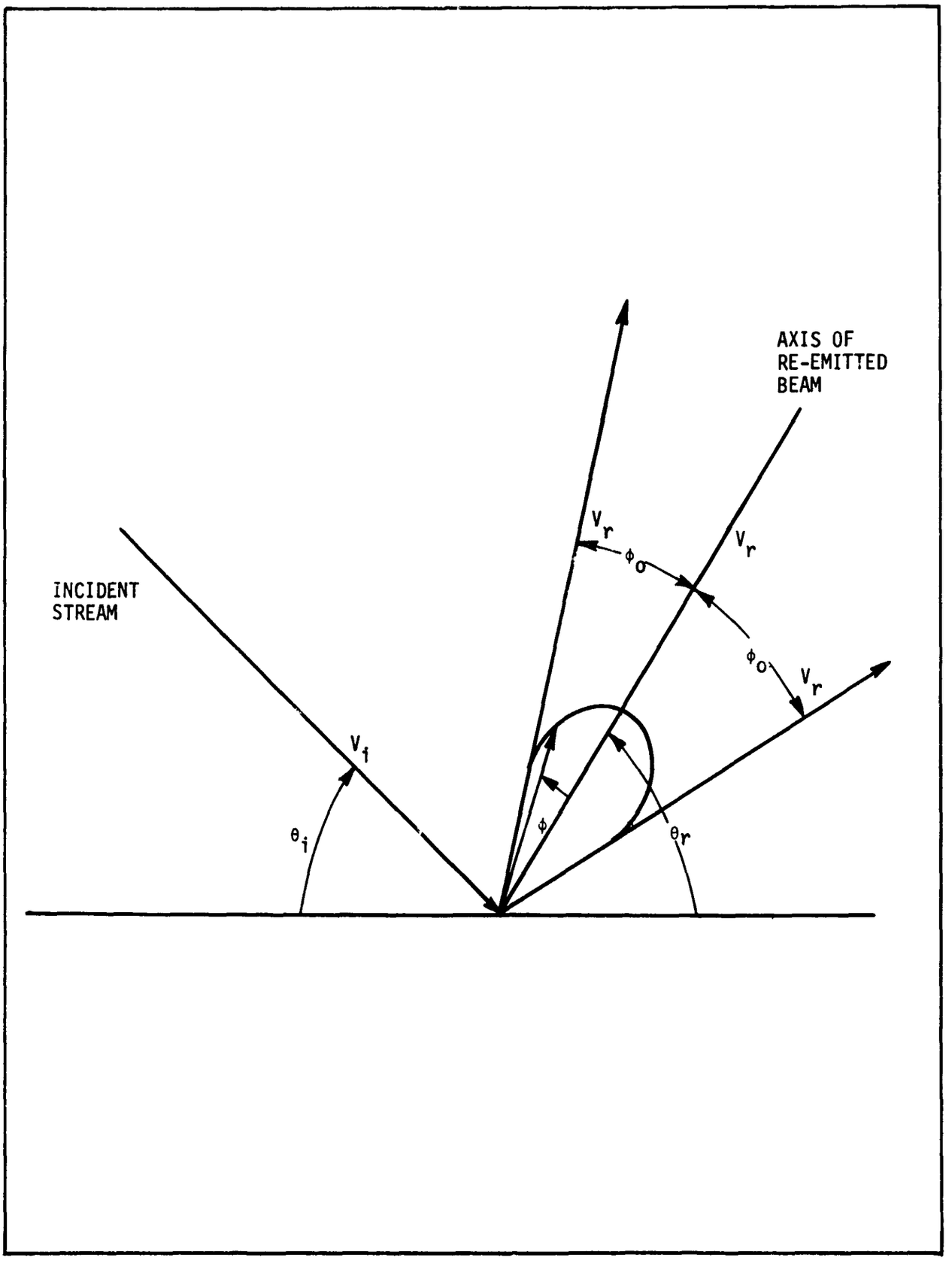

Figure C-1. SCHAMBERG'S SURFACE-PARTICLE INTERACTION MODEL (REF. 29)

where $\Phi(\phi_o)$ is the ratio of the axial momentum carried away to the momentum which would be carried away if all the particles in the beam were aligned with the beam axis (see Figure C-1). Graphs and formulas for $\Phi(\phi_o)$ are contained in Schamberg's papers (ref. 29).

Because only the paddles contribute to the spin drag, the value of f(ν, shape) was shown to be

$$f(\nu, \text{shape}) = \cos \delta \cos \eta \qquad \text{(C-4)}$$

as an average value per spin revolution of the satellite. The angle δ is the angle between the normal to a paddle surface and the spin vector, and η is the angle between the velocity vector and the spin axis at perigee.

Appendix D

METASTABLE STATES AND THE AUGER EFFECT

D.1 METASTABLE STATES

The basic state of any atom is stable since a spontaneous departure from this state is forbidden by the laws of quantum mechanics. The higher energy states of an atom are called excited states. The higher the energy of the orbit in which the electron is moving, the greater the excitation. When, after successive drops, the electron reaches its lowest energy level, all further radiation stops and the atom is said to be unexcited. The excited states of an atom however, are not stable since energy drops can occur spontaneously. Also, some theoretically possible energy drops are forbidden by quantum mechanics restrictions. Ergo, if all the drops from an excited level are forbidden, this level although excited, will be stable. These stable, excited levels are called metastable levels and their atom states are termed metastable states.

These metastable states can be eliminated by the appearance of incident light on the metastable state or by a collision. Either of these processes can move the electron to a higher energy level. Also collisions with the electron can occur where the electron loses energy. Then it will fall to a basic or lower energy level without radiating energy.

However, it has been proven experimentally that metastable states are not truly stable. These states have a mean lifetime of the order of 10^{-3} seconds, which is 10^{5} seconds longer than the average lifetime of many excited states. Therefore, the probability of dropping from a metastable state is considerably smaller than for many excited states.

In the kinetic theory of gases, the collisions between atoms occur so frequently that the majority of the atoms in metastable states are subjected to impacts before they have had time to radiate. Such impacts may excite these atoms to higher energy levels or may diminish their energy through collisions (those collisions which result in a loss, or transfer, of energy). Thus, the

drops from metastable states will be even more infrequent than they would normally be. A cold, rarefied gas (low temperature and pressure) is most favorable to the existence of metastable states.

The time of excitation, or the mean residence time in the excited state, can be used to determine whether or not a metastable state exists. The time of excitation, τ, is a function of the nature of the gas, its pressure, its temperature, and the size of the chamber. If τ ranges from 10^{-4} to 10^{-2} seconds, a metastable state of the electron exists. τ is usually much lower than 10^{-4} seconds for excited states.

Metastable states can ionize, excite, and dissociate other atoms and molecules by their ability to diffuse irrespective of the existing electric field. The populations in the excited state are expressed by

$$N' = N'_o \exp - (t/\tau)$$

where N'_o = number of electrons in the excited state which is reduced to N' after some time t. τ is the mean residence time in the excited state.

Atomic excitation is caused by (1) a collision of a fast particle (i.e., an electron) with the atom, (2) a collision of a photon with the atom (photo-excitation), and (3) a collision of the atom with an atom of higher temperature (thermal-excitation).

If the energy involved is higher than in any of the mechanisms causing atomic excitation, the collision may lead to ionization. In an ionization process, the electron becomes free and moves in a hyperbolic orbit.

The transitions of electrons between hyperbolic orbits, or from hyperbolic to elliptic orbits, or vice versa, result from the absorption or emission of radiation.

The most stable state is the ground state or lowest energy (maximum negative) state. The other states are either metastable or excited, and ionized.

Excitation of an atom results only if the collision satisfies certain quantum mechanics considerations including enough available energy for the transition. When the energy is equal to its critical value, the probability for excitation is zero. With increasing electron energy, the probability increases rapidly. The resonance state is related to the energy required to raise an electron from the ground state of an atom into the lowest excited state from which transitions back are optically permitted. The energy necessary to raise the electrons to metastable states from which transitions into the ground state are not permissible implies a probability. The probability of this event is the degree of metastability..

D.2 AUGER EFFECT

The gas-surface interaction experiment considered in this report involves the ejection of electrons from a metal detector surface following an impingement by a metastable molecule. In particular, a metastable N_2 molecule, which has passed through the collimator without a collision, will arrive in its excited state at the metal detector surface. Here the metastable molecule undergoes a radiationless decay (termed an "Auger Process") and ejects an electron from the metal.

If an ion or an excited atom approaches a metal surface, the ion may be neutralized and the excited atom may be de-excited or undergo resonance ionization (see Kaminsky, 1965, ref. 72). These processes are of particular interest in secondary electron emission and other phenomena. Four of the basic types of electronic transition which an incident ion or excited atom may undergo at a metal surface are resonance neutralization, resonance ionization, Auger de-excitation, and Auger neutralization. The neutralization process (ref. 72) is thought to consist of three steps:

(1) Resonance neutralization of the doubly charged ion to an excited state of the singly charged ion.

(2) Auger de-excitation of the excited singly charged ion to the ground state of the ion.

(3) Auger neutralization of the singly charged ion to the ground state of the atom.

Secondary electrons are emitted only in processes (2) and (3). The yield of secondary electrons per incident ion in (2) considerably exceeds the yield for process (3). Also, it is difficult to distinguish secondary electrons ejected by metastable atoms from those ejected by incident ions. Only by observing the maximum and minimum energies of the ejected electrons can this distinction be made.

In the Auger neutralization process of an ion at a metal surface, the electronic transitions involve two metal electrons from the conduction band. One metal electron neutralizes the incident ion directly to the ground state of the atom. The energy released in this transition causes another metal electron to be ejected from the metal surface.

Two processes allow electrons excited in an Auger neutralization process to leave the metal surface. On one hand, a certain fraction of the originally excited electrons have a large enough component of momentum normal to the metal surface to pass over the surface barrier and escape from the metal surface. However electrons can also escape by interactions with other metal electrons which may enable them to escape from the surface, indirectly over the surface barrier.

The final state of an Auger process has a finite lifetime because the electrons emitted in the Auger process leave holes in the filled portion of the conduction band, and these holes in turn are filled by secondary Auger processes involving electrons lying higher in the band (ref. 72).

The de-excitation of a metastable atom results from either a collision of the first kind (in which the metastable atom undergoes a transition into a higher energy level, after which it goes to the ground state by emission of radiation) or collisions of the second kind (in which the excitation energy is transmitted to the particle with which it collides and may cause the ejection of secondary electrons). The secondary electrons emitted in collision processes of the second kind may in turn result from two different processes. In one process the metastable atom will be converted into an ion and then undergo

Auger neutralization with electron emission. In another process the metastable atom will undergo Auger de-excitation also with electron emission (ref. 72).

The de-excitation of a metastable ion can consist of the Auger de-excitation process followed by Auger neutralization, which also leads to secondary electron emission. It is therefore possible to study the de-excitation processes of metastable atoms and ions by measuring the electron yield and the energy distribution of the secondary electrons.

In order to count only the secondary electrons emitted from metal surfaces being bombarded by metastable ions and atoms, it becomes necessary to discriminate against those electrons ejected by other effects. One contribution to the secondary electron current comes from photoelectrons resulting from radiation emitted in the de-excitation of metastable atoms and ions before they reach the target. Another unwanted source of secondary electrons is the interaction of unexcited singly charged ions (which are often present in the incident beam of metastable atoms or ions) with the target surface.

However, electrons ejected by singly charged metastable ions are more numerous and also have a higher kinetic energy than those ejected by singly charged ions in the ground state. This method of distinction, between the contribution to the total secondary electron current due to metastable particles and that due to the singly charged ions in the ground state, depends on the ability to detect the change in electron yield in response to the appearance of the metastable ions against the background of singly charged ions in the ground state.

The total yield of secondary electrons emitted from a metal surface under the impact of metastable noble gas atoms is close to the value of the total yield for singly charged ions in the ground state. This is understood since the metastable atom approaching the surface can be resonance ionized and subsequently Auger neutralized if the energy levels are appropriate. Thus the secondary electron emission due to primary ion bombardment should be almost completely indistinguishable from that due to ions formed by resonance ionization of a metastable atom within a critical distance from the surface.

Metastable noble gas atoms in interaction with metal surfaces undergo resonance ionization with subsequent Auger neutralization rather than Auger de-excitation.

In the experiment considered in this report an Auger detector surface is employed to study the electron yield from a metastable N_2 beam. Necessary precautions are taken to eliminate background ions and other particles which could influence the electron emission.

Appendix E

THE UNIVERSITY OF MICHIGAN GAS-SURFACE INTERACTION EXPERIMENT

E.1 THE TIME-OF-FLIGHT (TOF) VELOCITY DISTRIBUTION ANALYSIS

An interpretation of the detected metastable flux is best determined by considering a given beam of neutral particles with an arbitrary velocity distribution. Also a burst of electrons used to excite the neutral stream is used. The problem is to determine the metastable particle flux at a downstream detector as a function of time. Once this has been accomplished, the experimental problem of determining the velocity distribution from the metastable particle flux can be discussed.

The geometry considered for the neutral stream and electron beam is shown below.

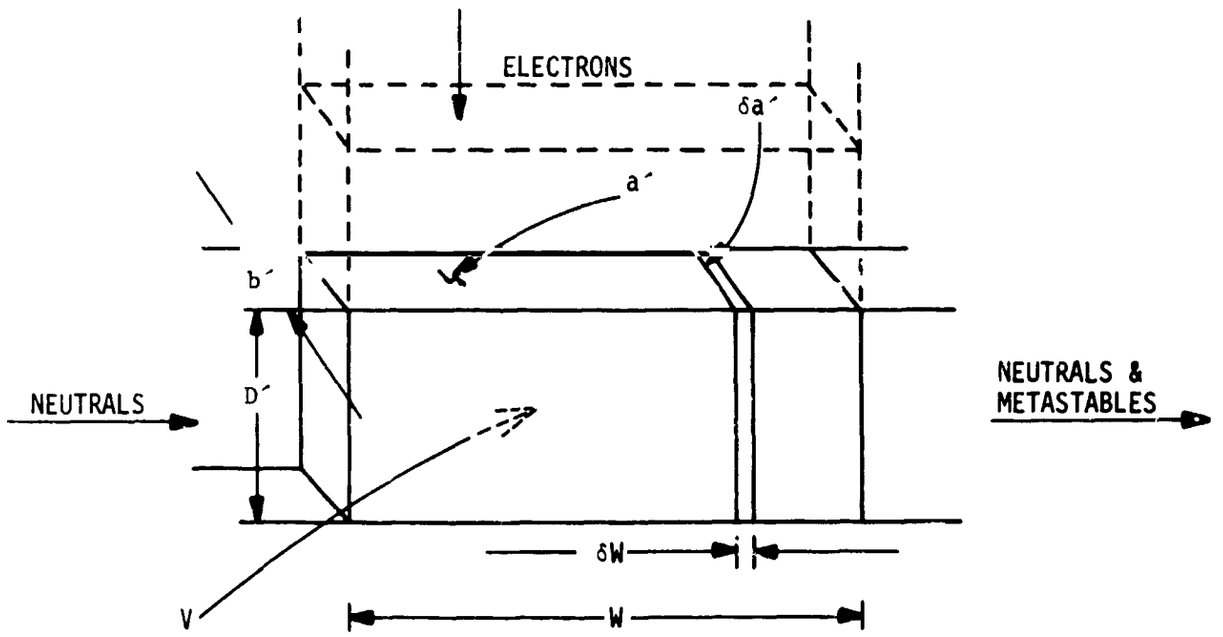

The following assumptions are made:

(1) The metastable lifetime is infinite (no metastable decay occurs over relevant time intervals).

(2) The fraction of the neutral beam which is metastabilized is negligible (the neutral particle density is constant over the region of excitation).

(3) The electron density is uniform over the cross-section of the electron beam.

(4) The electron pulse is rectangular in time (zero rise and fall times and constant over a time interval, τ).

(5) The metastable particles are undeflected by the electron bombardment (no recoil occurs).

The effects of the deviation from these assumptions on the interpretation of the detected metastable flux are discussed later.

First, consideration is given to an elemental Volume δV of the neutral beam as it drifts with its particles (of speed v) across the electron beam. From the preceding sketch,

$$\delta V = D' b' \delta W = D' \delta a'$$

If one electron per second crossed $\delta a'$, and if one neutral particle with excitation cross-section σ^* resides in δV, then the probability of excitation per unit time is $\sigma^*/\delta a'$ or, $\sigma^*/\delta a'$ metastables will be produced per second.

Also the resulting metastable density can be shown to be

$$\eta^* = \frac{\bar{i}}{e'} \frac{\sigma^*}{a'} \eta_o t = \beta t$$

where η_o is the neutral particle density, $\bar{i}$ the electron current, e' the electronic charge, and t represents the time that δV has been exposed to the electron beam. This expression enables us to determine the temporal behavior of the metastable particle density at any position along the emerging stream.

Another useful quantity is the transit time, T', of a neutral particle across the electron beam;

$$T' = \frac{W}{v}$$

where W is defined in the previous sketch and v is the neutral particle speed. The metastable density depends on whether this quantity is greater than or less than the time interval, τ, over which the electron beam is fired. $T'>\tau$ corresponds to slow neutrals. Here, some particles remain in the electron beam throughout its full firing interval. For these the maximum metastable density, $\beta\tau$, is achieved. In the second case, $t<\tau$ and no particles linger in the electron beam for its full duration. Thus its greatest possible metastable density is βt. Since all times are measured from the instant at which the electron beam is turned on, the metastable density at a collector located a distance L' from the edge of the electron beam can be determined. Also, the time the particles take to drift from the electron beam to the collector is determined as L'/v.

The metastable flux density at the collector as a function of time, the total number of metastables striking a unit area of the collector, and a normalized metastable flux density can be determined for both the slow neutrals ($v < \frac{W}{\tau}$) and the fast neutrals ($v > \frac{W}{\tau}$). The normalized flux is significant in that it provides the flux distribution associated with a single metastable particle. Hence, actual counting rates are obtained simply by scaling to the total number of metastables in the beam.

E.2 RESPONSE TO A NEUTRAL BEAM WITH ARBITRARY DISTRIBUTION OF PARTICLE SPEEDS

The electron beam can be considered to be a superposition of two hypothetical beams. At time t=0 an "excited" beam is turned on which produces metastables. At $t=\tau$, a "de-excited" beam, assumed to produce anti-metastables at the same efficiency as the previous beam, is turned on. Both beams are left running indefinitely. The superposition of these two beams is equivalent to no beam after $t=\tau$. Thus, only the response of the first case need be determined, since the total response is then obtained by subtracting from this the same result shifted by τ in time.

Then, considering only the excited beam, the metastable density at the collector, the metastable flux at the collector due to the exciting beam and the actual electron beam, and the normalized metastable flux can all be determined.

Also the drifting Maxwellian gas case can be considered. In this case, the velocities of the neutral gas particles follow the Maxwellian distribution law in a reference frame in which the gas is macroscopically at rest. The inclusion of a macroscopic drift term allows a description of the ambient gas flux to an instrument mounted on the satellite.

Additional consideration is given to simplification of the flux expression since it obscures the distribution function almost entirely. Secondly, the distribution function of the neutral gas must be inferred from the temporal behavior of the metastable flux. This is done by designing a system where $\frac{W}{L} << 1$ and $\frac{\tau}{t} << 1$.